

Universitätsklinikum Hamburg-Eppendorf

Institut für experimentelle Pharmakologie und Toxikologie

Prof. Dr. Thomas Eschenhagen

**Evaluation of the impact of microtubule modifications on
cMyBP-C and hypertrophic cardiomyopathy**

Dissertation

zur Erlangung des Grades eines Doktors der Medizin
an der Medizinischen Fakultät der Universität Hamburg

vorgelegt von:

Alexander Georgios Tourounoglou
aus Hamburg

Hamburg 2023

**Angenommen von der
Medizinischen Fakultät der Universität Hamburg am: 09.07.2024**

**Veröffentlicht mit der Genehmigung der
Medizinischen Fakultät der Universität Hamburg am:**

**Prüfungsausschuss, der/die Vorsitzende:
Prof. Dr. Catherine Meyer-Schwesinger**

**Prüfungsausschuss, zweite/r Gutachter/in:
Prof. Dr. Lucie Carrier**

Table of contents

1	Introduction	5
1.1.	Hypertrophic cardiomyopathy	5
1.2.	The sarcomere	9
1.3.	Cardiac myosin-binding protein C (cMyBP-C)	10
1.4.	Microtubules	12
1.5.	Aim of the study	15
2	Material and methods	17
2.1.	Animals	17
2.2.	<i>Mybpc3</i> -targeted knock-in (KI) mouse model	17
2.3.	Human Samples	17
2.4.	Isolation of adult mouse cardiomyocytes (AMCM)	18
2.4.1	Cultivation and treatment of AMCMs	21
2.4.2	Sample preparation	21
2.5.	Chemicals and solutions	22
2.6.	Antibodies	24
2.7.	Laboratory Equipment	27
2.8.	Western Blot analysis	28
2.8.1.	Sodium dodecyl sulfate polyacrylamide gel electrophoresis	28
2.8.2.	Western Blot (WB)	29
2.9.	Immunofluorescence	31
2.10.	Proximity ligation assay	33
2.13.	Statistical analysis	35
3	Results	36
3.1.	Validation of tubulin antibodies	36
3.1.1.	Validation for Western Blot	36
3.1.2.	Validation for immunofluorescence	37
3.2.	Quantification of dephosphorylated α -tubulin protein levels	39
3.3.	Investigation of dephosphorylated and phosphorylated α -tubulin after tubulin modifications	41
3.4.	Evaluation of protein-protein proximity	46
3.4.1.	Proximity of total α -tubulin and cMyBP-C	49
3.4.2.	Proximity of dephosphorylated α -tubulin and cMyBP-C	51
4	Discussion	53
4.1.	Quantity of dephosphorylated α -tubulin in HCM patients and mice	55
4.2.	Dephosphorylated α -tubulin and modifications	55
4.3.	Proximity Ligation Assay	57

4.4. Co-localization of α -tubulin and cMyBP-C.....	60
5 Summary	61
6 Zusammenfassung	63
7 Literature	65
8 Acknowledgements	70
9 Curriculum Vitae	72
10 Appendix	73
10.1. List of abbreviations	73
10.2. SI Prefixes.....	75
10.3. Protocol PLA Analysis	76
10.3.1. Analysis of cell area with ImageJ / FIJI	76
10.3.2. PLA signal count in ImageJ	76
11 Eidesstattliche Versicherung	78

1 Introduction

1.1 Hypertrophic cardiomyopathy

Diseases of the cardiovascular system remain with over 35% the leading cause of death in the general population in Germany (Figure 1).

Causes of death by chapter of ICD-10

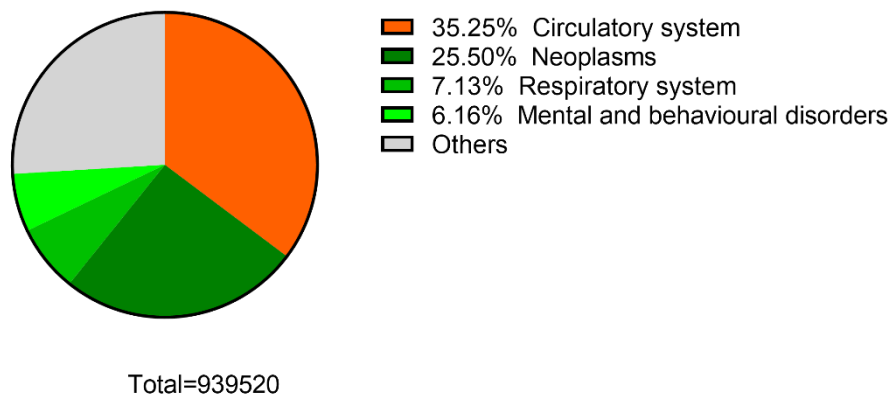


Figure 1: Causes of death by chapter of ICD-10 in Germany (2019). Over 35% of deaths in all genders in Germany were caused from diseases of the circulatory system. Numbers adapted from: Statistisches Bundesamt, visited: 2021.

Within the group of cardiovascular diseases cardiomyopathies play a relevant role. This specific subpopulation of cardiovascular diseases is characterized by structural and functional anomalies of the myocardium which cannot be explained by sole existence of coronary artery disease, hypertension, valvular disease, or congenital malformations (Elliott et al. 2008). Along the guidelines proposed by the 'European Society of Cardiology' (ESC) in 2008 cardiomyopathies are grouped according to certain morphological and functional criteria, with a subdivision into familial and non-familial forms (Figure 2).

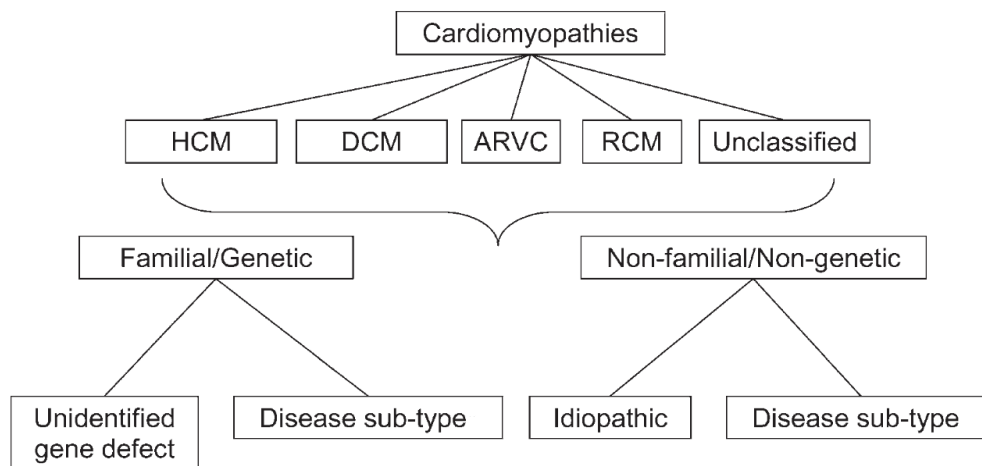


Figure 2: Classification of cardiomyopathies proposed by the European Society of Cardiology working group on myocardial and pericardial diseases, 2008. ARVC: arrhythmogenic right ventricular cardiomyopathy, DCM: dilated cardiomyopathy, HCM: hypertrophic cardiomyopathy, RCM: restrictive cardiomyopathy. (Elliot et al., 2008)

Among the different inherited myopathies of the heart, hypertrophic cardiomyopathy (HCM) is the most common form with an overall prevalence of 0.2% in the general population (Maron et al. 1995, McKenna and Judge 2021). Additionally, an age-related prevalence, with lower rates in patients under 25 years, was described (Zou et al. 2004). HCM can be defined by the appearance of increased ventricular wall thickness or mass in absence of loading conditions, such as valvular disease or hypertension, as reasonable cause leading to described myocardial conditions, though the diseases precise definition remains a topic of discussion (Elliott et al. 2008).

From a clinical perspective diagnosis of HCM can be challenging as many patients experience few, if any, symptoms. In this group, diagnosis is made by incidental or family screening. Other patients report a variable range of symptoms, most common are chest pain and dyspnea. Fewer patients sustain presyncopal conditions or syncope during exercise or at rest (Elliott and McKenna 2004). In infants, HCM causes signs of heart failure (HF) including tachypnea, excessive sweating, impaired feeding, and failure to thrive. Clinically, HCM is defined by increased left ventricular (LV) wall thickness ≥ 15 mm (in adults) in cardiac imaging techniques such as echocardiography, cardiac magnetic resonance imaging (cMRI) or computed tomography (CT). In some cases, HCM presents lesser degrees of wall thickening (13-14 mm) leading to diagnostic challenges when distinguishing disease from physiological state, such as hypertrophy found in some competitive athletes (Authors/Task Force et al. 2014). A further important characteristic is the diastolic dysfunction associated with this disease (Carrier 2021). Though not part of everyday clinical examination, histological changes in familial HCM can be detected. Main characteristics are myocyte disarray and accumulation of

interstitial fibrosis (Factor et al. 1991, Shirani et al. 2000). It is described that HCM can progress along different pathological pathways leading to progressive HF as cause of LV outflow obstruction (LVOTO), sudden cardiac death or atrial fibrillation with risk of stroke (Maron et al. 2014).

From a genetic standpoint HCM is an inherited disease with an autosomal dominant pattern. Mutations in at least 19 genes are described to be associated with the development of HCM encoding for components of the sarcomere. Among the different genes, *MYBPC3*, encoding cardiac myosin-binding protein C (cMyBP-C), and *MYH7*, encoding β -myosin heavy chain (β -MHC), are the most frequently associated with HCM (Schlossarek et al. 2011). *MYBPC3* is the leading HCM gene (Carrier et al. 2015). Over 60% of the known *MYBPC3* genetic variants are truncating, which include nonsense, splicing or branch point variants, insertions and deletions, all leading to C-terminally truncated cMyBP-C losing binding sites to titin and light meromyosin with a suggested impairment of function (Figure 4; (Schlossarek et al. 2011, Behrens-Gawlik et al. 2014). When compared to *MYH7*, a relevant number of *MYBPC3* genetic variants are associated with a more benign clinical course with later onset of symptoms and fewer cases of sudden cardiac death (Harris et al. 2011). Within individuals carrying a heterozygous truncating mutation haploinsufficiency appears to be the main mechanism of disease (Marston et al. 2012, van der Velden et al. 2015). Here, studies found lower levels of wild-type (WT) cMyBP-C without the detection of truncated protein (Marston et al. 2009).

Multiple mutations in an individual, however, are reported to be associated with a more severe manifestation of phenotype (Richard et al. 2003), with a relevant amount (14%) of HCM in children being caused by compound heterozygous *MYBPC3* genetic variants (Morita et al. 2008). Additionally, reported cases of homozygous and compound heterozygous individuals with bi-allelic truncating *MYBPC3* variants show an association with cardiomyopathy in neonates leading to HF with fatal outcome within the first year of life. Contrary to truncating mutations, missense genetic variants cause the assembly of stable mutant cMyBP-Cs that are integrated into the sarcomere and might act as poison polypeptides impairing sarcomere structure and function (for review see (Carrier et al. 2015)).

Besides the mutation itself many other factors such as environment, microRNAs and posttranslational modifications are supposed to influence the onset and the severity of the disease (Schlossarek et al. 2011).

Although clinical consequences of HCM are well described, current therapies remain only symptomatic and empirically based due to a lack of large, randomized trials (Authors/Task Force et al. 2014). The two main columns in HCM therapy are drug

therapy and surgery, with individual approaches depending on patients' symptoms and disease morphology. Pharmaceutical therapy relies mainly on treatment with non-vasodilating β -adrenoreceptor antagonists (β -blockers) or calcium (Ca^{2+})-channel blockers. Therapy with non-vasodilating β -blockers aims to lower cardiac workload and improve diastolic filling. Ca^{2+} channel blockers, such as Verapamil or diltiazem, come to use when therapy with β -blockers is contraindicated or inefficient and can improve symptoms by improvement of LV diastolic filling. Therapy of patients experiencing LVOTO aims to mitigate symptoms by pharmacological therapy, surgery, alcohol ablation or electrical pacing (Ommen et al. 2020). More recently, mavacamten, a selective inhibitor of cardiac myosin ATPase, was introduced as a novel therapeutic approach. By inhibition of actin-myosin cross-bridge formation mavacamten reduces contractility and thereby improves myocardial energetics (Anderson et al. 2018; Grillo et al. 2019). Clinical trials such as EXPLORER-HCM demonstrated its potential to ameliorate symptoms and mitigate LVOTO promises a highly targeted and pathophysiologically attuned approach in contrast to the symptomatic management which typifies conventional HCM therapy (Olivotto et al. 2020).

1.2. The sarcomere

A healthy adult resting heart rate ranges from 60 to 100 beats per minute. A heartbeat is the result of a harmonized contraction of cardiomyocytes which are the most common major cell type within atrial and ventricular tissue (Litvinukova et al. 2020). They contain dense cytoskeletal networks, amongst them the contractile sarcomeric cytoskeleton, organized into myofibrils, and the non-sarcomeric cytoskeleton, made of β - and γ -actin, microtubules, and intermediate filaments (Caporizzo et al. 2019). A myofibril is composed of repeating sections of thick and thin myofilaments, called sarcomeres, which form a contractile unit within a myocyte. According to the nomenclature of microscopic anatomy, a sarcomere can be defined as the structure between two neighboring Z-discs. Located in between the Z-lines are the I-band, mainly composed of the thin filaments, and the A-band, mostly containing the bipolar thick filaments (Figure 3). The A-band encompasses the C-Zone, where cMyBP-C is located, and the M-band, as cross-link for myosin filaments. Fixation proteins, such as α -actinin, link the sarcomeres to each other and the sarcolemma. Thin filaments are mainly made of globular actin molecules which express specific binding sites for myosin, which are covered by tropomyosin. Additionally, troponin a complex of three protein subunits (cardiac troponin T (cTnT), cardiac troponin I (cTnI), and cardiac troponin C (cTnC)), is part of the thin filaments. The thick filaments are made of bipolar myosin, a family of adenosinetriphosphate (ATP)-dependent motor proteins, known for their role in actin-based motility during muscle contraction and intracellular transport. They consist of heavy chains (α - β -MHC) with a head domain and light chains with essential and regulatory function. The myosin's head domain binds to actin and moves along the thin filament by force generated from ATP hydrolysis. Thick filaments are stabilized and connected to the Z-discs by a giant protein, called titin. It is the largest protein known, composed of 27,000 amino acids, spans from the Z-disc to M-band, and contributes to the elasticity of the contracting muscle.

The interaction of actin and myosin, leading to shortening of the sarcomere and therefore myocyte contraction, is dependent of intracellular Ca^{2+} concentration. Following myocyte depolarization, intracellular Ca^{2+} concentration increases and Ca^{2+} ions bind to cardiac troponin C (cTnC), which leads to a conformational change of tropomyosin. This allows actin-myosin binding and initiates the ATP-dependent cross-bridge cycling with migration of myosin head domains along the actin filaments, in sum leading to myocyte contraction. When the stimulus is removed, intracellular Ca^{2+} concentration is actively decreased by a variety of mechanisms, such as the sarco/endoplasmic reticulum Ca^{2+} -ATPase (SERCA) or a sodium-calcium exchanger (NCX) at the sarcolemma. The actin binding site is covered up by tropomyosin as Ca^{2+} is no longer bound to cTnC, and the contraction cycle ends.

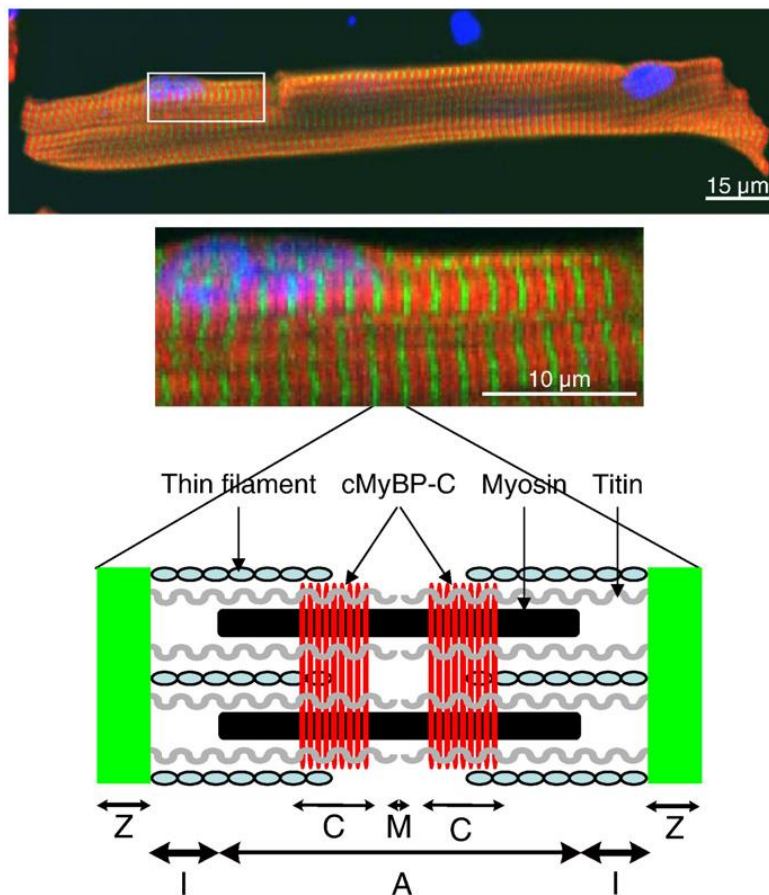


Figure 3: Visualization of cardiac myosin-binding protein C (cMyBP-C) in the sarcomere of an adult mouse ventricular myocyte. Top: Immunofluorescence analysis of an isolated adult mouse cardiomyocyte. Antibodies targeted cMyBP-C (red, C-Zone in A-Band) and α -actinin (green, Z-disc). Nuclear staining was performed with TopPro3® (blue). Middle: Higher magnification of rectangular (white bordered) area in top image. Visualization of cMyBP-C doublets within the A-band, flanked by single α -actinin bands. Bottom: Schematic depiction of a sarcomere in between two Z-discs. Thick filaments, including myosin and cMyBP-C, are intertwined with thin filaments, including globular actin molecules, tropomyosin, and the troponin complex. Titin with its elastic properties is shown as the third sarcomeric component. Within the A-band, the C-Zone and the M-line are located. The I-band is shown between A-band and Z-disc. Figure adapted from (Schlossarek et al. 2011).

1.3. Cardiac myosin-binding protein C (cMyBP-C)

Cardiac myosin-binding protein C (cMyBP-C) is a thick filament-associated protein in the cardiac sarcomere which participates in the preservation of sarcomeric structure and regulation of contraction and relaxation (Carrier et al. 2015). Within the sarcomere it is located in the C-Zone of the A-Band (see Figure 3), an area of crossbridges between myosin and actin (Winegrad 1999). The cMyBP-C protein has a molecular weight of 150 kDa and is exclusively expressed in the heart (Fougerousse et al. 1998). There are two other isoforms known, a fast-skeletal and a slow-skeletal muscle MyBP-C (Yamamoto and Moos 1983). The cardiac protein is encoded by the *MYBPC3* gene, found on chromosome 11p11.2, and consists of over 21000 bp, with 35 exons, of which 34 are

coding. The entire sequence of a human *MYBPC3* gene was first described by Lucie Carrier and colleagues (Carrier et al. 1997). The cMyBP-C protein is composed of eight immunoglobulin-like and three fibronectin-like domains (see Figure 4). In contrast to skeletal isoforms, the cardiac isoform expresses specific regions such as a N-terminal C0-domain and the MyBP-C motif (M-Motif) with multiple phosphorylation sites. Via multiple subdomains cMyBP-C interacts with different fractions of the sarcomere. Towards the N-terminal end potential interaction sites with actin are described as well as an interaction with the S2 fragment of myosin via the M-Motif (see Figure 4). The C-terminal domain interacts with titin and light meromyosin (LMM; (Schlossarek et al. 2011)).

Regarding its quaternary structure different models have been proposed, while the precise formation is not entirely understood yet. Most models suggest a trimerization of cMyBPC molecules to form a collar-like structure around the thick filament backbone. Here the C5-C10 domains bind to myosin and the C-terminal end orient towards the periphery to interact with actin and the S2-domain of myosin (Winegrad 1999, Moolman-Smook et al. 2002, Schlossarek et al. 2011).

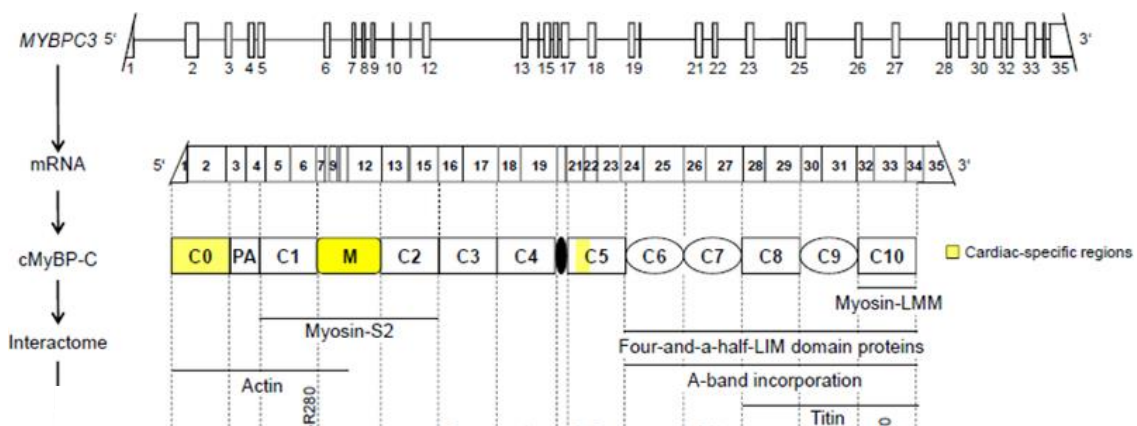


Figure 4: Schematic depiction of MYBPC3, transcribed mRNA and cMyBP-C with interaction sites. MYBPC3 comprises 21 kbp and consists of 35 exons, transcribed into a 3824-bp transcript. The final protein, cMyBP-C, is composed of 8 immunoglobulin-like (C0, C1, C2, C3, C4, C5, C8, C10) and 3 fibronectin-like (C6, C7, C9) domains. Depicted in yellow are the cardiac-specific regions, as contrast to slow- and fast-skeletal isoforms of cMyBP-C. The M-Motif (M), as potential interaction site with myosin-S2 is located between the C1 and C2 domains. Further, there are interaction sites with F-actin (C0-M). Via the C6 to C10-domains cMyBP-C interacts with the C-Zones of the A-bands of the sarcomere. At the C-terminus interaction sites with titin (C8-C10) and light meromyosin (LMM, C10) are located. Figure adapted from (Carrier et al. 2015).

Further studies have shown an important role of cMyBP-C within the relaxation process of myocytes. By maintaining myosin in super-relaxed state therefore allowing a full relaxation of cardiomyocytes in the diastole, as functionally impaired cMyBP-C leads to residual cross-bridge cycling in diastole, incomplete relaxation as well as increased Ca^{2+} -sensitivity of myofilaments. Additionally, cMyBP-C was found to interact with myosin and

actin at the peak of myocyte contraction. Thus, a loss or impairment of function, for example through mutation, can lead to a much faster contraction and early relaxation (Pohlmann et al. 2007).

1.4. Microtubules

Microtubules are cytoskeletal filaments that fulfill a variety of roles within a cell such as internal organization, structural support, chromosomal segregation, and intracellular trafficking (Goodson and Jonasson 2018). They are highly dynamic polymers made of α - and β -tubulin heterodimers that form hollow tubes. Microtubules are ever-changing structures, with constant addition and subtraction of tubulin dimers at both ends. However, the change at either end is not balanced, as one end, the plus (+) end, undergoes more rapid changes in contrast to the other, the minus (-) end. This creates a heterogeneous, highly dynamic population of microtubules which are constant subject to cycles of polymerization and depolymerization, both *in vivo* and *in vitro* (Janke and Bulinski 2011). This form of turnover is known as dynamic instability and was first described in 1984 (Mitchison and Kirschner 1984). The flexibility in morphology is essential for the creation of contacts between microtubule ends and target organelles, for example during mitosis. In proliferating animal cells, most microtubules are organized by the centrosome, the main microtubule-organizing centre (MTOC). It allows a proper formation and positioning of the bipolar spindle apparatus during mitosis (Prosser and Pelletier 2017). Along the differentiation to perform organ specific functions, the microtubule network re-organizes with the formation other subcellular microtubule organization sites, termed non-centrosomal MTOCs (ncMTOCs) (Sanchez and Feldman 2017). In cardiomyocytes specifically in the perinuclear region (Zebrowski et al. 2015).

Factors which influence the probability of microtubule polymerization and depolymerization remain subject of current investigations. However, a variety of enzymes and binding proteins are proposed to influence the equilibrium between microtubule growth and disassembly (Akhmanova and Steinmetz 2008).

Considering the variety of microtubule functions and interactions within a cell, it appears essential to coordinate their properties for a well-organized cellular homeostasis. Therefore post-translational modifications (PTMs) emerged as possible regulators of microtubule properties and assembly (Janke and Bulinski 2011). Specifically, the tyrosination and detyrosination of α -tubulin at the C-terminal microtubule is at interest. By removing the C-terminal tyrosine microtubules are indirectly stabilized as microtubule depolymerizing kinesins from the kinesin-13 family favorably depolymerize tyrosinated

microtubules (Janke and Bulinski 2011). By preventing disassembly detyrosination is associated with an increase in microtubule network density and suggested to suppress contractility by amplifying myocardial stiffness. It was shown that increased detyrosination leads to an increase in cross-linking of microtubules with intermediate filaments and sarcomeric proteins, such as desmin, which act as a sarcomeric anchor for the microtubule network (Kerr et al. 2015).

The process of detyrosination was first observed in 1975 and later shown to be reversible (Arce et al. 1975, Hallak et al. 1977). The tyrosination at the C-terminal microtubule is catalyzed by a tubulin-tyrosine ligase (TTL) (Raybin and Flavin 1977). Within the cell the TTL tyrosinates soluble tubulin dimers, therefore the majority of newly formed microtubules appear in the tyrosinated state (Gundersen et al. 1987). Detyrosination is mediated by a long suspected but just recently discovered tubulin tyrosine carboxypeptidase, an enzymatic complex of vasohibin 1/2 (VASH1/2) and its chaperone, the small vasohibin-binding protein (SVBP) (Aillaud et al. 2017). It was also shown that this enzyme complex is the tubulin carboxypeptidase (TCP) responsible for microtubule detyrosination in cardiomyocytes. Here the complex of VASH1/SVBP inherits a predominant role as *VASH1* gene expression was shown to be ≈ 28 - to 50-fold higher than *VASH2* expression all causes of HF, in this study HCM, DCM and ischaemic HF. Interestingly, no significant changes in the *VASH1* gene expression were observed when comparing HCM to NF (Chen et al. 2020).

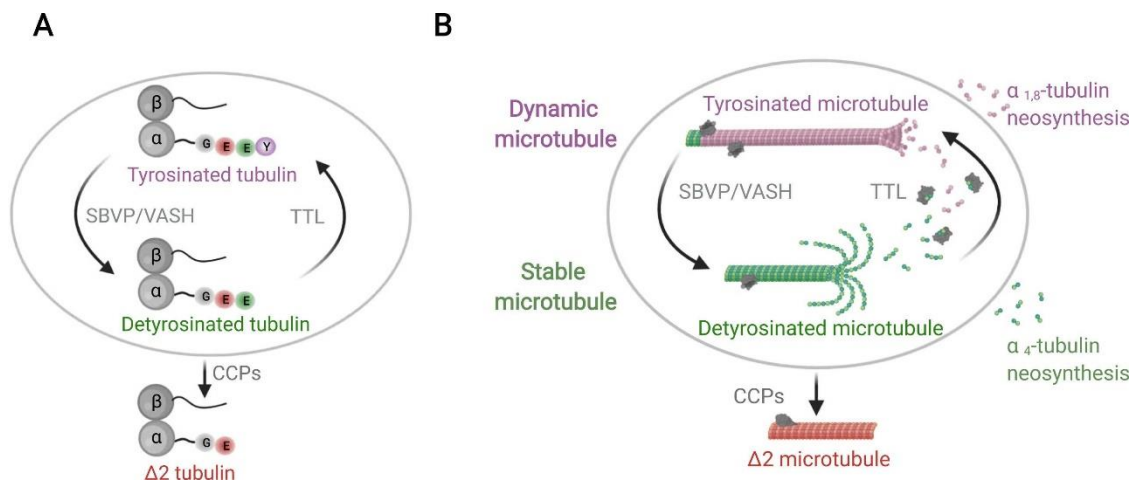


Figure 5: Schematic depiction of MYBPC3, transcribed mRNA and cMyBP-C with interaction sites. (A) Schematic representation of $\alpha\beta$ tubulin dimer with the C-terminal tails, representation with the last 4 amino acids at the C-terminal tail of α -tubulin. Tubulin carboxypeptidases (TCPs), here VASH1 or VASH2 together with SVBP, remove the C-terminal tyrosine residue (Y, in purple) of α -tubulin to create detyrosinated tubulin. Via the tubulin tyrosine ligase (TTL), which can add a tyrosine residue at the C-terminal glutamate (E, in green), detyrosinated tubulin can be re-tyrosinated. By removal of the penultimate glutamate residue (E, in green) detyrosinated tubulin can also permanently leave the cycle. This is moderated by cytosolic carboxypeptidases (CCPs), generating $\Delta 2$ -tubulin. (B) Schematic representation of modified microtubule subpopulations and corresponding enzymes of the cycle acting on either microtubules or soluble dimers. TCPs preferably act on tyrosinated microtubules (purple) to create detyrosinated microtubules (green). After microtubules depolymerize, TTL acts on soluble dimers. After polymerization of these soluble dimers tyrosinated microtubules are created (purple) representing the dynamic newly formed microtubules in cells. In long-lived detyrosinated microtubules, CCPs create $\Delta 2$ microtubules (red). Figure adapted from (Sanyal et al. 2023).

Besides the physiological modulations there are a variety of chemicals known to promote or inhibit different PTMs at the C-terminal end of the microtubule. Parthenolide (PTL) a sesquiterpene lactone was shown to inhibit the activity of the TCP and therefore decreases portion of detyrosinated α -tubulin in vitro without altering the total density of the microtubule network (Fonrose et al. 2007). Paclitaxel (or Taxol®) a tubulin targeting drug used in chemotherapy was shown to stabilize the microtubule network and the proportion of detyrosination of microtubules while not altering the total microtubule content (Kerr et al. 2015).

Next to dynamic microtubules there is a subgroup of stable microtubules within the cytoskeleton. These are required for cellular morphogenesis as they provide a structural backbone for a variety of cellular subpopulations and can act as compression-bearing struts (Kirschner and Mitchison 1986, Baas et al. 2016). In striated muscles, a stable microtubule network is described as a relevant factor determining cytoskeletal stiffness with a sinusoidal deformation of longitudinally oriented microtubules under compression (Kerr et al. 2015, Robison et al. 2016). This buckling behavior suggests the existence of anchor points for microtubules within the sarcomere. Among others, the intermediate filament desmin has been suggested to act as sarcomeric anchor for microtubules, with

an affinity to detyrosinated tubulin. This appears consistent with findings which claim an abundance of detyrosinated microtubules leads to suppressed contractile velocity and increased myocardial stiffness (Kreitzer et al. 1999, Robison et al. 2016). Whether desmin remains the solitary sarcomeric anchor for the microtubule network, especially for detyrosinated tubulin, remains unclear.

Recent studies in human HF identified a central role for detyrosinated microtubules in regulating cardiomyocyte function. An increase in detyrosination was shown to correlate with impaired myocardial function in animal (rat) models of heart disease (Belmadani et al. 2002, Kerr et al. 2015). Furthermore, higher protein levels of detyrosinated tubulin were detected in patients with diagnosed hypertrophic and dilated cardiomyopathy (Schuldt et al. (2021). HCM patient data showed an inverse correlation between LV ejection fraction (LVEF), a clinical marker for contractility, and abundance of detyrosinated tubulin, while tyrosinated or total tubulin levels showed no such correlation. A reduced expression of TTL in HCM patients could not be shown (Robison et al. 2016). On the other hand, knockdown of VASH1 or overexpression of TTL resulted in a lower myocardial stiffness and an increase relaxation speed in cardiomyocytes from HF patients (Chen et al. 2020). This supports the idea of a further therapeutic target for patients with impaired diastolic function. Whether detyrosinated microtubules behave similarly in murine HCM models and interact with further sarcomeric anchors remains topic of further investigation, paving the way for this work.

1.5. Aim of the study

Mutations in the *MYBPC3* gene were shown to play an essential role in the pathophysiology of HCM, both in human and mice (Vignier et al. 2009, Schlossarek et al. 2011)

Current therapies for HCM, despite the just recently approved mavacamten, mainly focus on relieve of symptoms and the prevention of sudden cardiac death but there remains further need for therapy strategies targeting the cause of HCM. Our group has worked on different therapy approaches for HCM caused by *MYBPC3*-mutations and found promising results with gene therapy, correcting mutations by 5'-*trans*-splicing molecules (Mearini et al. 2013), oligonucleotide-mediated exon skipping (Gedicke-Hornung et al. 2013) and insertion of an intact, unmutated *MYBPC3* gene (Mearini et al. 2014) in HCM

mice. These approaches aim to preclude the manifestation of HCM in the first place. However clinical application remains in the future.

More recent studies suggest a relevant role of the microtubule network, especially the detyrosination of tubulin, in regulation of myocardial function and manifestation of HCM in human and animal models (Kerr et al. 2015, Robison et al. 2016). Causes for this alteration of microtubule formation remain unclear.

To further investigate the role of cMyBP-C in the pathomechanisms leading to the development of HCM and possible interactions with the microtubule network, the goal of this thesis was to answer the following questions:

1. Are protein levels of detyrosinated tubulin altered in samples from human HCM patients and a HCM mouse model?
2. Can tyrosination and detyrosination of tubulin be modified in isolated cardiomyocytes?
3. Is there evidence for an interaction between the microtubule network, especially detyrosinated tubulin, and cMyBP-C suggesting it as a potential novel sarcomeric anchor? And if so, can the interaction be altered by paclitaxel (microtubule stabilizer) and parthenolide (microtubule destabilizer) treatment?

The findings can provide a more thorough understanding of the role of cMyBP-C in HCM and might be a steppingstone for the identification of further causal therapy approaches in the future.

2 Material and methods

2.1. Animals

Animal care and procedures were performed in accordance with the Guide for the Care and Use of Laboratory Animals published by the US National Institute of Health (Publication No. 85-23, revised 1985).

2.2. *Mybpc3*-targeted knock-in (KI) mouse model

Our group created a *Mybpc3*-targeted knock-in (KI) mouse model carrying a point mutation on the last nucleotide of exon 6 within the *Mybpc3* gene (Vignier et al. 2009). The chosen variant location was based on the most frequent founder variant within the *Mybpc3* gene found in a screening study in Italy (Girolami et al. 2006). Using the Cre/lox system for gene targeting, the G>A transition on the last nucleotide of exon 6 was introduced leading to the expression of three different mRNAs: Missense (exchange of G for A), nonsense (exon skipping, frameshift, PTC) and deletion/insertion (as nonsense but with additional partial retention of downstream intron, restoring of the reading frame, almost full-length protein) and furthermore lower levels of mRNAs of *Mybpc3*. In fact, total mRNA levels were found to be 80% lower in homozygous KI mice compared to wild-type (WT) (Vignier et al. 2009). The homozygous KI mice exhibit phenotypic characteristics of HCM such as LV enlargement, increased heart/body weight ratio, reduced fractional area shortening, increased interstitial fibrosis as well as increased myofilament calcium sensitivity and diastolic dysfunction. In sum, the resulting hypertrophy and reduced left-ventricular function are a suitable model for the HCM phenotype (Vignier et al. 2009, Fraysse et al. 2012, Mearini et al. 2013). WT and KI mice were bred on a Black Swiss genetic background.

2.3. Human Samples

Human cardiac tissue samples were collected from HCM patients with *MYBPC3* mutations undergoing septal myectomies, non-failing human hearts not suitable for transplantation or organ donors which died from a non-cardiac cause (Thottakara et al. 2015). Materials from patients and donors were collected with informed consent of the

donors with approval of the local ethical boards and according to the Declaration of Helsinki.

2.4. Isolation of adult mouse cardiomyocytes (AMCM)

The isolation of adult mouse cardiomyocytes (AMCMs) by retrograde perfusion with recombinant collagenases was performed using a previously described and established protocol in the group of Prof. Dr. Lucie Carrier (O'Connell et al. 2007, Pohlmann et al. 2007).

To prevent blood clotting during preparation and perfusion mice were intraperitoneally injected with Heparin (200 units) at least 15 minutes prior starting the protocol. This was followed by CO₂-anesthesia and cervical dislocation to sacrifice the animal. Thereafter the thorax was opened, and the ascending aorta was dissected and cut about 5 mm cranial of the heart's base. The heart was then extracted from the body, mounted on a cannula with the help of two fine curve-tip forceps and fixed with a thread. The cannulated heart was then attached to a Langendorff perfusion system which was heated to 37 °C, and perfused in retrograde direction with a specific perfusion buffer at a flow rate of 4 mL/min. To suppress cardiac contraction during procedure the perfusion buffer contained the myosin inhibiting substance 2,3-butanedione monoxime (BDM) and was free of Ca²⁺ ions. After 2 minutes of perfusion, clearing the vascular system from any remains of blood and cellular detritus, the perfusion buffer was replaced by a digestion buffer. This buffer contained a mixture of different collagenases and other enzymes to dissociate the AMCMs from their surrounding connective tissue. The heart was perfused for 9 minutes with the digestion buffer then ventricles were separated from the organ and caught in a small porcelain dish which contained 2.5 ml digestion buffer and Stop 1 solution. This mixture brought the digestion to a hold as fetal calf serum (FCS) in the Stop 1 solution inhibited the enzymatic breakup of the cardiac tissue. The ventricles were then manually dissected using a small pair of scissors and forceps. When homogenized the cell mixture was transferred into a tube using a wide mouth pipette. Any solid remains in the porcelain dish were again mixed with Stop 1 solution, homogenized manually, and transferred into a second tube where the mixture was sedimented for 30 to 45 seconds. The supernatants from tube 1 and 2 were transferred into a third tube and sedimented for 10 minutes. For optimized AMCM yield the cell pellets in tube 1 and 2 were mixed with Stop 2 solution, sedimented for 30 to 45 seconds and the supernatants were then transferred into a fourth tube followed by another 10 minutes of sedimentation. The supernatants of tube 3 and 4 were carefully removed, leaving the vivid AMCMs behind, which were then resuspended in Stop 2 solution. Both alloys were then conveyed to a

plastic dish where calcium concentration was successively increased by adding CaCl₂ reaching a final concentration of 1 mM over 10 minutes. The final cell yield was then counted in a Fuchs-Rosenthal chamber (3.2 µL per chamber) and calculated by the following equation:

$$Total\ cell\ count = \frac{Cell\ count\ per\ chamber\ side}{Volume\ of\ chamber\ side} \times$$

Volume of cardiomyocyte suspension

After 30 minutes of sedimentation in a Falcon reaction tube, the supernatant (Stop 2 solution and cell detritus) was removed, and myocytes were resuspended in freshly prepared cell culture medium (MC-CM) and ready for further experiments.

MC cell culture medium (MC-CM, final volume 50 ml)

Bovine serum albumin (100 mM)	0.05 ml (final concentration 0.1%)
Insulin-Transferrin-Selenium (ITS, 100 mM)	0.5 ml (final concentration 1%)
Penicillin/Streptomycin (100 mM)	0.5 ml (final concentration 1%)
MEM (+ Hank's salts, + L-Glutamin)	ad 50 ml

Stock Perfusion buffer (final volume 500 ml)

NaCl (3000 mM)	18.84 ml (final concentration 3.77%)
KCl (1000 mM)	2.45 ml (final concentration 0.49%)
KH ₂ PO ₄ (500 mM)	0.6 ml (final concentration 0.12%)
Na ₂ HPO ₄ -2H ₂ O (500 mM)	0.6 ml (final concentration 0.12%)
MgSO ₄ -7H ₂ O (500 mM)	1.2 ml (final concentration 0.24%)
NaHCO ₃ (1000 mM)	6 ml (final concentration 1.2%)
KHCO ₃ (1000 mM)	5 ml (final concentration 1%)
4-(2-hydroxyethyl)-1-piperazineethanesulfonicacid (HEPES) buffer (1000 mM, pH 7,46)	5 ml (final concentration 1%)
Taurine (500 mM)	30 ml (final concentration 6%)
Milli Q water	ad 500 ml

Perfusion buffer

Glucose (500 mM)	5,55 ml (final concentration 1.11%)
BDM (500 mM)	10 ml (final concentration 2%)
Penicillin/Streptomycin (100 mM)	5 ml (final concentration 1%)
Stock perfusion buffer	ad 500 ml

Digestion buffer

CaCl ₂ -2H ₂ O (100 mM) 0.01%)	0.0043 ml (final concentration
Liberase TM (5 mg/ml, ROCHE)	0.525 ml (final concentration 1.5%)
Perfusion buffer	ad 35 ml

Stop 1 solution

Bovine calf serum (100 mM)	1 ml (final concentration 1%)
CaCl ₂ -2H ₂ O (100 mM) 0.13%)	0.0125 ml (final concentration
Perfusion buffer	ad 10 ml

Stop 2 solution

Bovine calf serum (100 mM)	1 ml (final concentration 0.5%)
CaCl ₂ -2H ₂ O (100 mM)	0.025 ml (final concentration 0.13%)
Perfusion buffer	ad 20 ml

2.4.1 Cultivation and treatment of AMCMs

To induce tubulin modifications freshly harvested AMCMs were suspended in MC-CM and transferred to a 12-well plate using a wide-mouth pipette to avoid damage of the cells. Each well was loaded with 2 ml of cell suspension and treatments were added as follows. For paclitaxel treatment, 2 μ l of paclitaxel stock (10 mM) were added to reach a final concentration of 10 μ M in each well. The parthenolide treatment was introduced in a similar way, adding 2 μ l of parthenolide stock (10 mM) to the cell suspension to reach a final concentration of 10 μ M in each well. As a control, 2 μ l of DMSO were added to other wells. The cells were then incubated for 2 hours under cell culture conditions (37 °C, 21% O₂, 2% CO₂, humidity > 90%). After treatment the medium was removed, and cells were washed once with 1 ml MC-CM per well and fixed with 4% PFA as described above.

2.4.2 Sample preparation

First tissue samples for protein analysis were powdered, then protein extraction was performed in two steps. The tissue powder (30 μ g) was dissolved in 150 μ l water which included a protease inhibitor mixture (complete mini™, Roche Diagnostics). This was followed by three free-thaw-cycles and tissue homogenization by using the Tissue Lyser (2 x 30 s at 20 Hz). Then, product was centrifuged at 4 °C at maximum speed for 30 min in a table-top centrifuge. The supernatant was kept as the cytosolic fraction. In a next step, the pellet was homogenized in 240 μ l SDS-buffer (3% SDS, 30 mM Tris-base, pH 8.8, 5 mM EDTA, 30 mM NaF 10 % glycerol and 1 mM DTT) and centrifuged at room temperature with maximum speed for 10 min in a table-top centrifuge. The supernatant was again kept as the fraction for further protein analysis.

For protein analysis of AMCS, were cultivated in 100 μ l MC-CM for 2 hours under cell culture conditions (see 2.4.1), then washed once with 100 μ l MC-CM and then frozen at -20 °C in a mix of 100 μ l MC-CM, 1 ml Kranias buffer and 1 μ l DTT (1 mM). Before measurement samples were thawed and centrifuged at room temperature with maximum speed for 10 minutes in a table-top centrifuge.

Protein concentrations finally were determined with the Qubit® 3.0 Fluorometer (Life technologies) according to manufacturer protocol.

2.5. Chemicals and solutions

Product	Manufacturer
2,3-butanedione monoxime (BDM)	Sigma/Merck
Acetic Acid	Carl Roth
Acrylamide/Bis 40%	Bio-Rad
Amersham™ ECL™ Prime	GE Healthcare
Ammonium persulfate (APS)	Bio-Rad
Amplification stock buffer	Sigma-Aldrich (PLA Kit)
Bovine serum albumin (BSA)	Sigma/Merck
Bromphenol Blue	Sigma
Calcium chloride (CaCl ₂)	Roth
Di-sodium hydrogen phosphate (Na ₂ HPO ₄)	Merck
Dithiothreitol (DTT)	Carl Roth
Dulbecco's phosphate-buffered saline (DPBS)	Merck
Duolink PLA Probe MINUS	Sigma-Aldrich (PLA Kit)
Duolink PLA Probe PLUS	Sigma-Aldrich (PLA Kit)
EDTA (Triplex III)	Carl Roth
Fetal calf serum	gibco® by life technologies™
Glucose	Merck
Glycerol	Merck
Glycine	Carl Roth
HCl 37% fuming	Merck
HEPES	Roth
ITS-X solution (51 500-056)	Gibco® by life technologies™
Laminin	Roche
Liberase™	Roche
Ligase	Sigma-Aldrich (PLA Kit)
Ligation stock buffer	Sigma-Aldrich (PLA Kit)
Magnesium sulfate (MgSO ₄)	Merck
Methanol	J. Baker
Milk powder	Carl Roth

Minimum Essential Medium (MEM, 1X, +Hank's Salts, +L-Glutamine)	Gibco® by life technologies™
Mowiol 4-88	Hoechst
Paclitaxel (T7402-1MG)	Sigma-Aldrich
Parthenolide (P0667-5MG)	Sigma-Aldrich
Penicillin/Streptomycin	Gibco® by life technologies™
Polymerase	Sigma-Aldrich (PLA Kit)
Ponceau S solution	Sigma
Potassium chloride (KCl)	Merck
Potassium hydrogen carbonate (KH ₂ PO ₄)	Merck
Potassium hydrogen carbonate (KHCO ₃)	Merck
Precision Plus Protein TM Dual Color Standard	Bio-Rad
Qubit® Protein Assay Kit	Life technologies
Sodium chloride (NaCl)	Merck
Sodium dodecyl sulfate (SDS)-pellets	Carl Roth
Sodium hydrogen carbonate (NaHCO ₃)	Merck
Super Signal West Dura	Pierce
Taurine	Sigma/Merck
Tetramethyl ethylenediamine (Temed)	Bio-Rad
Tris base	Sigma
Triton X-100	Sigma
Tween 20	Sigma
Wash Buffer A	Sigma-Aldrich (PLA Kit)
Wash Buffer B	Sigma-Aldrich (PLA Kit)

2.6. Antibodies

Western Blot:

Primary antibodies

Detected Protein	Primary antibody	Manufacturer	Dilution
cMyBP-C	MyBPC3 (F-1), sc-137181, Mouse monoclonal	Santa Cruz	1:1000
Detyrosinated α -tubulin	Detyrosinated α -tubulin (J63), rabbit polyclonal	Gift from M. Moutin, Grenoble	1:2000
S6	S6 Ribosomal Protein (5G10) #2217, rabbit monoclonal	Cell Signaling	1:500
β -tubulin	Anti-beta (beta31), mouse monoclonal	Gift from M. Moutin, Grenoble	1:2500
Total α -tubulin	Total α -tubulin (α 3A1), mouse monoclonal	Gift from M. Moutin, Grenoble	1:5000
Tyrosinated α -tubulin	Tyrosinated α -tubulin (Y1/2), rat monoclonal	Gift from M. Moutin, Grenoble	1:5000
α -actinin	α -actinin (A7811), mouse monoclonal	Sigma	1:20000
Δ 2-tubulin	Δ 2-tubulin (J63 delta2), rabbit polyclonal	Gift from M. Moutin, Grenoble	1:5000

Secondary Antibodies

Secondary Antibody	Manufacturer	Dilution
Anti-Mouse IgG	Sigma	1:10000
Anti-Mouse IgG	Dianova	1:20000
Anti-Rabbit IgG	Sigma	1:6000

Anti-Rat IgG	Dianova	1:10000
--------------	---------	---------

Immunofluorescence:

Primary antibodies

Detected Protein	Primary antibody	Manufacturer	Dilution
cMyBP-C	Anti-MYBPC3 (Ab171153), Rabbit polyclonal	Abcam	1:100
cMyBP-C	MYBPC3 (F-1) sc-137181, Mouse monoclonal	Santa Cruz	1:100
Connexin-43	Connexin-43, BD 610061, mouse monoclonal	BD Biosciences	1:100
Desmin	Desmin, SAB5600054, Rabbit monoclonal	Sigma-Aldrich	1:500
Detyrosinated α -tubulin	Detyrosinated α -tubulin (J63), rabbit polyclonal	Gift from M. Moutin, Grenoble	1:1000
Dystrophin	Dystrophin, ab15277, rabbit polyclonal	Abcam	1:100
Lamin A/C	Lamin A/C, mouse monoclonal	Gift from A. Bertrand, Paris	1:100
LC3	LC3, #2775, rabbit polyclonal	Cell Signaling	1:200
Titin M8/M9	Titin, rabbit polyclonal	Gift from S. Labeit, Heidelberg	1:200
Total α -tubulin	Total α -tubulin, (α 3A1), mouse monoclonal	Gift from M. Moutin, Grenoble	1:5000
Tyrosinated α -tubulin	Tyrosinated α -tubulin (Y1/2), rat monoclonal	Gift from M. Moutin, Grenoble	1:200
α -actinin	α -actinin (A7811), mouse monoclonal	Sigma	1:200

Secondary antibodies

Secondary Antibody	Manufacturer	Dilution
Anti-Mouse IgG, Alexa Fluor 488 (LT A11029)	Life Technologies	1:600
Anti-Mouse IgG, Alexa Fluor 546 (LT A11030)	Life Technologies	1:600
Anti-Rabbit IgG, Alexa Fluor 488 (LT A11034)	Life Technologies	1:600
Anti-Rabbit IgG, Alexa Fluor 546 (LT A11035)	Life Technologies	1:600

Proximity ligation assay:

Primary antibodies

Detected Protein	Primary antibody	Manufacturer	Dilution
cMyBP-C	Anti-MYBPC3 (Ab171153), Rabbit polyclonal	Abcam	1:100
cMyBP-C	MYBPC3 (F-1) sc-137181, mouse monoclonal	Santa Cruz	1:100
Connexin-43	Connexin-43 BD 610061, mouse monoclonal	BD Biosciences	1:100
Desmin	Desmin, SAB5600054, rabbit monoclonal	Sigma-Aldrich	1:500
Detyrosinated α -tubulin	Detyrosinated α -tubulin (J63), rabbit polyclonal	Gift of M. Moutin, Grenoble	1:1000
Dystrophin	Dystrophin (ab15277), rabbit polyclonal	Abcam	1:100
Lamin A/C	Lamin A/C, mouse monoclonal	Gift from A. Bertrand	1:100
LC3	LC3, #2775, rabbit polyclonal	Cell Signaling	1:200
Titin M8/M9	Titin, rabbit polyclonal	Gift from S. Labeit, Heidelberg	1:200

Total α -tubulin	Total α -tubulin (α 3A1), mouse monoclonal	Gift of M. Moutin, Grenoble	1:5000
α -actinin	α -actinin (A7811), mouse monoclonal	Sigma-Aldrich	1:200

2.7. Laboratory Equipment

Blotting paper (Whatman 3MM)	Schleicher & Schuel
ChemiDoc™ Touch Imaging System	Bio-Rad
Comb 10 well 1,0 mm	Bio-Rad
Comb 15 well 1,0 mm	Bio-Rad
Coverslips (10 mm)	Glaswarenfabrik Karl Hecht KG
Culture plates (12-well)	Nunc
Culture plates (6-well)	Nunc
Falcon tubes (15 and 50-ml)	Sarstedt AG & Co.
Glassware	Schott Duran
Microscope slides	Paul Marienfeld
Mini Trans-Blot Electrophoretic Transfer Cell	Bio-Rad
Mini-Protean Tetra Cell	Bio-Rad
Nitrocellulose membrane	Schleicher & Schuel
Parafilm® M	Sigma-Aldrich
Petri dish (10 cm Diameter) + Lid	Sarstedt
Pipette tips (for 10, 100, 1000 μ l pipettes)	Sarstedt AG & Co.
PowerPac Basic Power Supply	Bio-Rad
Qubit® 3.0 Fluorometer	Life technologies
Serological pipettes (1, 2, 5, 10, 25, 50 ml)	Eppendorf
Short plates	Bio-Rad
Spacer plates 1,0 mm	Bio-Rad
Vacuum filtration rapid filtermax (100, 250, 500 ml)	TPP®
Zeiss Axio Observer Z1 / 7	Zeiss

2.8. Western Blot analysis

For Western Blot analysis, a standard protocol from the group of Prof. Dr. Lucie Carrier was used. In advance prepared protein samples were initially measured for their protein concentration using the Qubit® 3.0 Fluorometer (Life Technologies) with the Qubit® Protein Assay Kit (Life technologies).

2.8.1. Sodium dodecyl sulfate polyacrylamide gel electrophoresis

For protein analysis the sodium dodecyl sulfate polyacrylamide gel electrophoresis (SDS-PAGE) method is used. The SDS covers up intrinsic charges of individual proteins, forming micellar structures, which then migrate through a polyacrylamide gel when an electric field is applied. By denaturing the proteins and covering the intrinsic charges the SDS-PAGE method allows the separation of single proteins solely by their molecular mass.

Proteins were dissolved in 1x Laemmli buffer and then separated on 12 % polyacrylamide gels by electrophoresis. The polyacrylamide gel was divided into an upper stacking gel and a lower separating gel. Electrophoresis was initiated with 80 V for 10 minutes, then at 150 V for 80 to 90 minutes to fully separate the protein mixture in a 1x electrophoresis buffer. The Precision Plus Protein™ Dual Color Standard was used as a molecular weight marker and helped to monitor the progress of the electrophoresis.

Laemmli buffer (6x)

SDS	1.2 g
Bromphenole blue	6 mg
Glycerol	6 g
Tris base (0.5 M, pH 6.8)	1.2 ml (final concentration 12%)
DTT	0.93 g
Milli Q water	ad 10 ml

Stacking gel (final volume 10 ml)

Acrylamide/bis solution (29:1, 40%)	1.28 ml (final concentration 5.12%)
Tris base (0.5 M, pH 6.8)	2.5 ml
SDS	0.1 ml (final concentration 10 %)
APS	0.1 ml (final concentration 10 %)
TEMED	0.01 ml (final concentration 0.01%)
Milli Q water	6.03 ml

Separating gel (12% acrylamide concentration, final volume: 10 ml)

Acrylamide/bis solution (29:1, 40%)	3 ml (final concentration 12%)
Tris base (1,5 M, pH 8.8)	2.5 ml
SDS	0.1 ml (final concentration 10%)
APS	0.1 ml (final concentration 10%)
TEMED	0.004 ml (final concentration 0.4%)
Milli Q water	4.3 ml

Electrophoresis buffer (10x)

250 mM Tris-base	30.2 g
1.92 M Glycine	144 g
SDS	10 g (final concentration 1%)
Milli Q water	ad 1000 ml

2.8.2. Western Blot (WB)

When fully separated, the proteins were transferred to a nitrocellulose membrane by wet blotting at 300 mA for 90 minutes at 4 °C in a Mini Trans-Blot Electrophoretic Transfer Cell using a transfer buffer (1x Blot buffer II). To verify a successful transfer of protein onto the membrane, staining with Ponceau S was performed. After washing 3x 5 min with 1x TBS-T, membranes were blocked for at least 1 hour at room temperature using

either 5% milk powder solution or 5% BSA (for tubulin antibodies). Then, membranes were introduced to the primary antibody solution and incubated overnight at 4°C under subtle movement. The next morning, after washing 3x 5 min, the membrane was incubated with the secondary antibody solution and incubated for 1 hour at room temperature. Following a final washing step with 1x TBS-T, blotting detection was performed using the ECL-Prime Kit according to the instruction manual. To detect chemiluminescent signals the ChemiDoc™ Touch Imaging System was used and detected signals were processed and quantified with the Image Lab software (Bio-Rad).

When additional staining of the membrane was needed, antibodies were removed from the membrane using the Restore™ PLUS Western Blot Stripping Buffer (Thermo Scientific). After application of 5 ml stripping buffer membranes were incubated at room temperature for 30 minutes under subtle movement. Following the incubation, an additional blocking step was performed, and new antibody solutions were added as described above.

Blot buffer II (5x)

Tris-base (250 mM)	58 g
Glycine (1.9 M)	290 g
SDS	10 g (final concentration: 0.5%)
Milli Q water	ad 2000 ml

TBS (10x)

Tris-base	121.1 g
NaCl	87.66 g
HCl (37%)	adjust pH to 7.5
Milli Q water	ad 1000 ml

TBS-Tween (1x, 0.1%)

10x TBS	100 ml
Tween 20	1 ml
Milli Q water	900 ml

Milk powder solution (5%)

Milk powder (not fat, dry (blotting grade))	2.5 g
1x TBS-Tween (0.1%)	50 ml

Bovine serum albumin (BSA, 5%)

BSA	2.5 g
1x TBS-Tween (0.1%)	50 ml

2.9. Immunofluorescence

For further antibody staining, treatment and analysis AMCMs were fixed on a coverslip. Therefore, a glass coverslip (\varnothing 1 cm) was placed on the bottom of a 12-well plate, covered with 600 μ l laminin solution and incubated under cell culture conditions at 37 °C for at least one hour. The laminin solution was then removed and 1 ml of MC-MC with around 40,000 freshly harvested AMCMs was added to the wells and incubated under cell culture conditions (37 °C, 21% O₂, 7% CO₂, humidity > 90%). After two hours of incubation viable myocytes were attached to the cover slip while loose and deceased cells were removed in a washing step using 1ml MC cell culture medium. For final fixation 1 ml of 4 % paraformaldehyde was added for 10 minutes to the wells, followed by two washing steps with phosphate buffered saline (PBS).

The immunofluorescence analysis itself was performed using an established protocol from Prof. Carrier's working group. At first, 1 ml of blocking solution (Solution A) was added to each well and incubated for 45 minutes at room temperature. The coverslips were then transferred to a sheet of laboratory film and washed twice with 100 μ l of Solution B for 10 minutes total. Following the washing step primary antibodies and 100 μ l of Solution B were added and incubated over night at 4 °C. After incubation, two washing steps with Solution B for 5 minutes were performed. Secondary antibodies and DRAQ5™ (1:1000) for nucleus staining were diluted in Solution B and 100 μ l of antibody

solution was added to the coverslips. Incubation was performed for 45 minutes at room temperature protected from light. In the next step, AMCMs were washed three times in 1x PBS for 15 minutes total protected from light and transferred to object slides (cells facing towards downwards) adding Mowiol 4-88 (Sigma-Aldrich) in between. Using the Zeiss Axio Observer microscope with a 40x-oil objective and a Zeiss LSM 710 system confocal images were obtained.

Laminin solution

Laminin	100 μ l (final concentration 2%)
PBS	ad 5 ml

Solution A

FCS	500 μ l (final concentration 10%)
BSA	250 μ l (final concentration 1%)
Triton X-100	25 μ l (final concentration 0.5 %)
PBS (1x)	4225 μ l

Solution B

BSA	1.5 ml (final concentration 1%)
Triton X-100	150 μ l (final concentration 0.5%)
PBS (1x)	28.35 ml

Paraformaldehyde (4%)

Paraformaldehyde (20%, Thermo Scientific)	10 ml
Milli Q water	40 ml

2.10. Proximity ligation assay

For the proximity ligation assay (PLA) experiments on AMCMs a protocol was established adapted from the standard Duo Link® PLA Fluorescence protocol (Sigma-Aldrich). Reagents which were used in the protocol were prepared according to Duo Link® PLA Fluorescence.

AMCMs previously isolated from WT and KI mice and fixed on coverslips (as described previously) were placed on Parafilm® inside a petri dish and covered with a corresponding lid. The coverslips were then blocked with 1 ml Solution A per well for one hour at room temperature to reduce unspecific antibody binding. This was followed by two washing steps for 5 minutes each with 1 ml of Solution B under mild agitation. Following the washing step, primary antibody solutions (100 µl per coverslip) were added and incubated over night at 4 °C. The following day the primary antibody solution was removed, coverslips were washed twice for 5 minutes with 1 ml Wash Buffer A and cells were covered with 80 µl Duolink® PLA Probe Solution (Duolink® PLA Probe A and B) per coverslip and incubated under cell culture conditions (37 °C, 21% O₂, 7% CO₂, humidity > 90%) for one hour. After incubation with the PLA probes the supernatant solution was removed, cells were washed twice with Wash Buffer A and ligation was initiated by applying 80 µl of ligation solution to each coverslip. Cells were then incubated for 30 minutes under cell culture conditions. Ligation solution was discarded, and coverslips were washed twice for 2 minutes in Wash Buffer A. To initiate the amplification of the PLA product 80 µl of amplification solution were added to each coverslip and incubated for 100 minutes under cell culture conditions. This and the following steps were performed protected from light, according to the protocol. To finalize the experiment, amplification solution was removed, and coverslips were washed twice for 10 minutes with Wash Buffer B and once with Solution B, all under slight agitation in a 12-well plate.

For improved visualization the PLA was followed by an immunofluorescence staining of α -actinin in the sarcomere and the nucleus (via 4',6-diamidino-2-phenylidole (DAPI)) as described above. To finalize the procedure a microscope slide was covered with a drop of Mowiol 4-88, coverslips with AMCMs were mounted on top and the edges were sealed with nail polish.

To quantify the visual PLA results a protocol was established using the public domain software 'ImageJ' with the 'FIJI' image processing package. In brief, the area of signals generated in the PLA was compared to the total cell area providing a ratio of signal per cell area. The detailed protocol can be found in the appendix of this thesis.

Solution A

FCS	500 µl (final concentration 10%)
BSA	250 µl (final concentration 1%)
Triton X-100	25 µl (final concentration 0.5 %)
PBS (1x)	4225 µl

Solution B

BSA	1.5 ml (final concentration 1%)
Triton X-100	150 µl (final concentration 0.5%)
PBS (1x)	28.35 ml

PLA Probe Solution

Duolink® PLA Probe Plus	176 µl
Duolink® PLA Probe Minus	176 µl
Solution B	528 µl

Ligation buffer (1x)

Ligation Stock buffer (5x)	176 µl
ApoH ₂ O	704 µl

Ligation Solution

Ligase (1 U/µl)	22 µl
Ligation Buffer (1x)	858 µl

Amplification buffer (1x)

Amplification Stock buffer(5x)	176 μ l
ApoH ₂ O	704 μ l

Amplification solution

Polymerase (10 U/ μ l)	11 μ l
Amplification buffer (1x)	869 μ l

2.13. Statistical analysis

All acquired data were shown as mean \pm SEM. Statistical analysis was performed using Graph Pad Prism 6. Comparison in the same group was done using the unpaired Student's t-test.

Multiple groups were analyzed by a one-way ANOVA analysis with Bonferroni post-test. Values of $p < 0.05$ was considered statistically significant and were marked with a single, values of $p < 0.01$ were marked with two asterisks and values of $p < 0.001$ were marked with three asterisks.

3 Results

MYBPC3, encoding cMyBP-C, is the most frequently mutated gene leading to the expression of HCM. To this day the understanding of the disease remains incomplete due to missing knowledge regarding the extent of pathological alterations on cellular level. Recent insights hint towards the importance of microtubule dynamics and tubulin posttranslational modifications in cardiomyopathy (Kerr et al. 2015, Robison et al. 2016). Detyrosination of α -tubulin is a marker of stabilized microtubules and increases cardiomyocyte stiffness, but a detailed analysis of the interplay between components of the sarcomere and microtubules remains to be evaluated.

3.1. Validation of tubulin antibodies

Prior to further investigations tubulin antibodies targeting different subtypes of the microtubule network were tested and validated for the main methods used in this study. Results of this validation process will be shown in the following.

3.1.1. Validation for Western Blot

For antibody validation in Western Blot analysis the tubulin antibodies were tested on protein lysates isolated from cardiac tissue healthy human donors and HCM patients as well as from murine ventricular tissue (MVT) and AMCMs. Western Blot was performed according to the protocol (see 2.8.) and primary antibodies directed against different subtypes of tubulin, were tested in different dilutions (data not shown). The antibodies targeting total α -tubulin (α 3A1), detyrosinated tubulin (J63), tyrosinated tubulin (Y1/2) and total β -tubulin (beta31) produced specific bands at the expected molecular weight (see Figure 6).

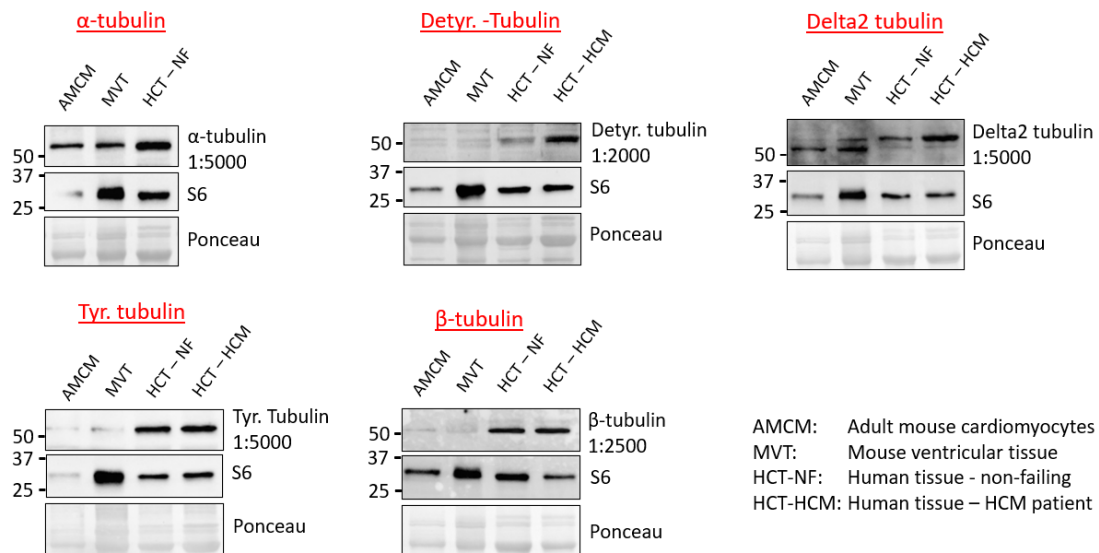


Figure 6: Validation of tubulin antibodies for Western Blot analysis. Tubulin antibodies were tested on protein lysates isolated of adult mouse cardiomyocytes (AMCM), mouse ventricular tissue (MVT), human cardiac tissue of non-failing hearts (HCT-NF) and cardiac tissue of HCM patients (HCT-HCM). The ribosomal S6 kinase and the Ponceau were used as loading control. All tubulin antibodies bands appear at the expected fragment size of 52 kDa. Delta2 tubulin antibody stained a second band slightly above 55 kDa in MVT and human samples.

Antibodies targeting detyrosinated tubulin produced lower protein staining in healthy tissue samples (AMCM, MVT and non-failing human cardiac tissue) compared to tissue from human HCM patients. Both tyrosinated tubulin and β -tubulin produced lesser signal in murine than in human tissue. The antibody targeting Delta2-tubulin produced unspecific signals, staining targets at different molecular weights (above the 55 kDa marker) in human and mouse and was therefore not used in the following experiments.

3.1.2. Validation for immunofluorescence

After showing specificity for most tubulin antibodies in Western Blot analysis, tubulin antibodies were tested for immunofluorescence analysis. Therefore, AMCMs were isolated from WT mice and stained with primary tubulin antibodies according to the immunofluorescence protocol (see 2.9.). Antibodies targeting total α -tubulin, detyrosinated and tyrosinated tubulin produced an immunofluorescence signal in a microtubule shape with an accentuated signal around the nucleus (see Figure 7). Immunofluorescence with the antibody targeting Delta2-tubulin produced considerable amounts of unspecific background signal (data not shown) and was therefore not used for further analysis. The antibody targeting detyrosinated tubulin generated less extensive fluorescence signal when compared to other tubulin antibodies in AMCMs (see Figure 7, C). However, signal intensity in locations around the nucleus appeared comparable to findings in other antibody testing. For verification and improved

visualization, a second primary antibody was added to each immunofluorescence analysis targeting a sarcomeric protein, either α -actinin or cMyBP-C (see Figure 7, B – C).

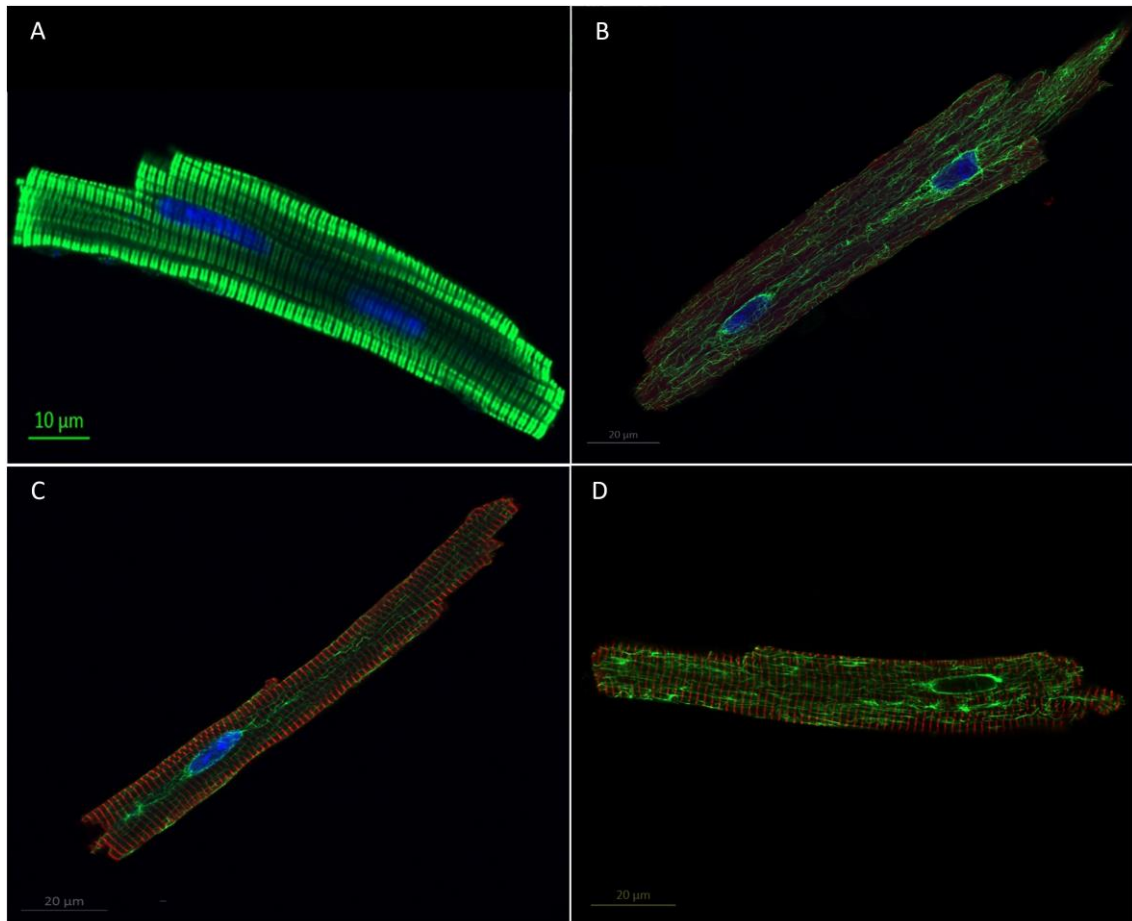


Figure 7: Antibody validation for immunofluorescence. The immunofluorescence was performed on adult mouse cardiomyocytes isolated from WT mice. In (A) cMyBP-C (green) and the nucleus (blue, DAPI) were stained. Image (B) shows staining of total α -tubulin (green), a sarcomere staining for cMyBP-C (red) and the nucleus (blue, DAPI). In (C) detyrosinated α -tubulin (green), α -actinin (red) and the nucleus (blue, DRAQ5) were targeted. Image (D) visualizes tyrosinated tubulin (green) and α -actinin (red) and the nucleus (blue, DRAQ5). For (A) scale 10 μm , for (B) – (D) scale 20 μm .

3.2. Quantification of detyrosinated α -tubulin protein levels

To obtain an improved understanding of microtubule modifications and their role in HCM, protein levels of tubulin subtypes were analyzed by Western Blot in cardiac tissue samples from human healthy donors or HCM patients and from WT and KI mice.

At first protein levels total α -tubulin were measured in human cardiac tissue by Western Blot (Figure 8).

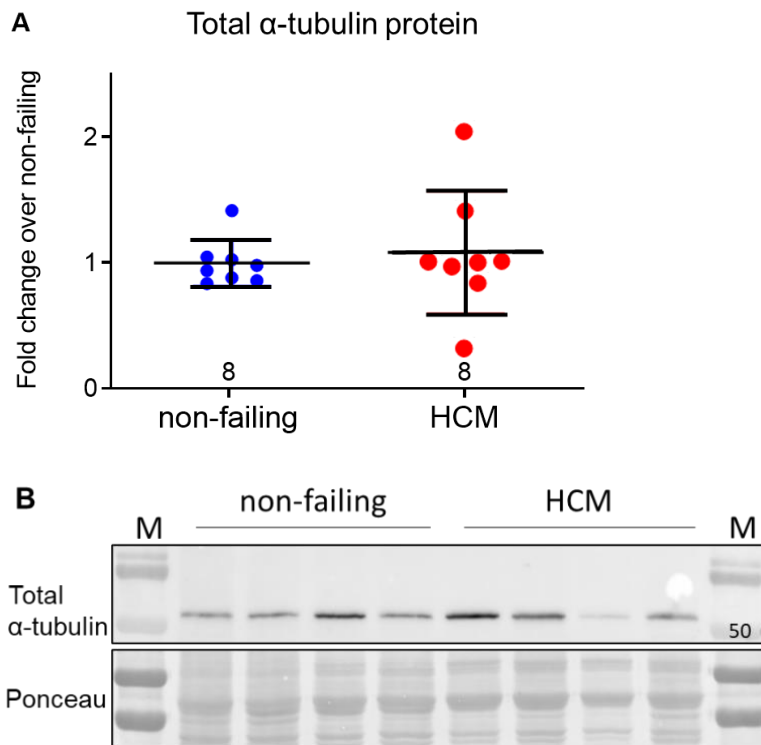


Figure 8: Protein levels of total α -tubulin in human non-failing and HCM hearts. (A) Quantification of total α -tubulin protein levels in myectomies from human non-failing hearts (NF) and patients with hypertrophic cardiomyopathy (HCM). Ponceau was used as loading control. No significant difference was found. (B) Representative Western blots of indicated proteins in samples from human non-failing (NF) and HCM hearts. Expected molecular weight: total α -tubulin: 52 kDa. M = molecular weight marker. Data are expressed as mean \pm SEM, unpaired t-test, N = 8.

After quantification and normalization to a loading control data showed no significant in protein levels of total α -tubulin in tissue derived from patients expressing HCM in comparison to the non-failing group (Figure 8, A).

Then protein levels of detyrosinated tubulin were measured in a similar sample set (Figure 8).

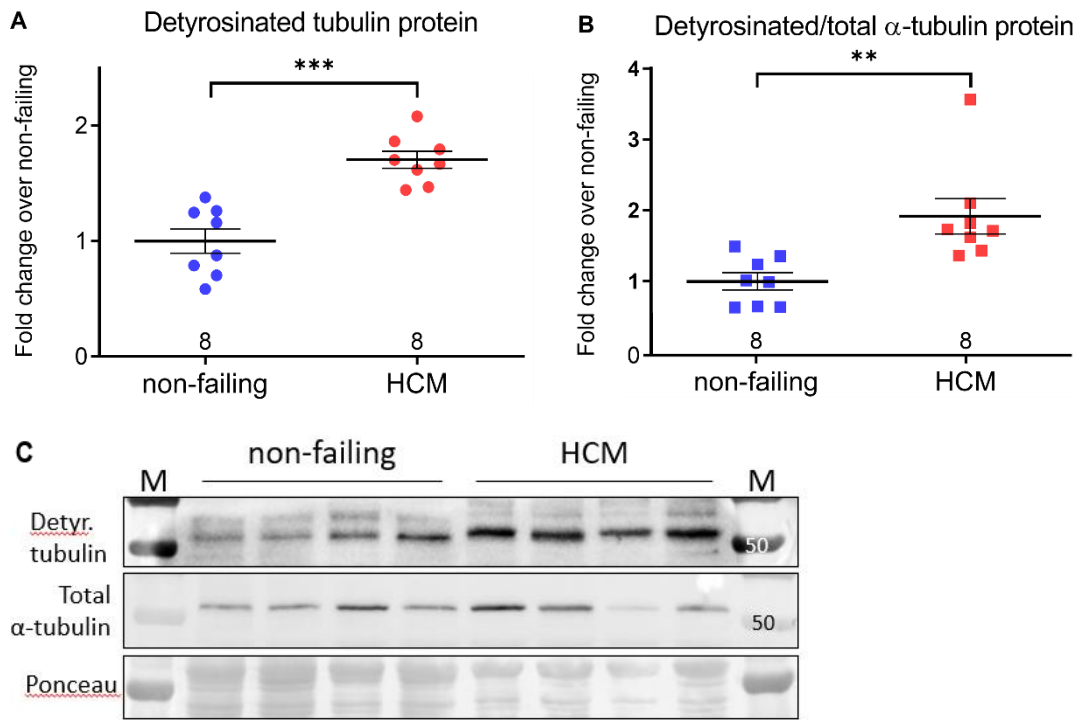


Figure 9: Protein levels of detyrosinated tubulin in human non-failing and HCM hearts. (A) Quantification of detyrosinated tubulin protein levels in myectomies from human non-failing hearts (NF) and patients with hypertrophic cardiomyopathy (HCM). Ponceau was used as loading control. (B) Quantification of detyrosinated tubulin to total α -tubulin ratio in non-failing and HCM myocardial tissue. (C) Representative Western blots of indicated proteins in samples from human non-failing (NF) and HCM hearts. Expected molecular weight: detyrosinated tubulin: 52 kDa, total α -tubulin: 52 kDa. M = molecular weight marker. Data are expressed as mean \pm SEM with ** p <0.01; *** p <0.001, unpaired t-test, N = 8.

After quantification and normalization to a loading control data showed higher protein levels of detyrosinated α -tubulin in tissue derived from patients expressing HCM in comparison to the non-failing group (Figure 9, A). In addition, protein levels of total α -tubulin were measured in the same groups. No significant difference in between both groups was found (data not shown).

To determine the change in proportion, a ratio between detyrosinated and total α -tubulin protein levels was created. Combined data showed a 1.9-fold higher detyrosinated/total α -tubulin ratio in HCM patients than NF (see Figure 9, B).

After evaluation of protein levels of detyrosinated α -tubulin in human HCM, the same protein analysis was performed in the HCM mouse model. Therefore, cardiac tissue samples from *Mybpc3*-targeted knock-in (KI) mice were analyzed by Western Blot and compared to samples from WT mice (Figure 10, B). In addition, protein levels of total α -tubulin were quantified in both groups (Figure 10, C).

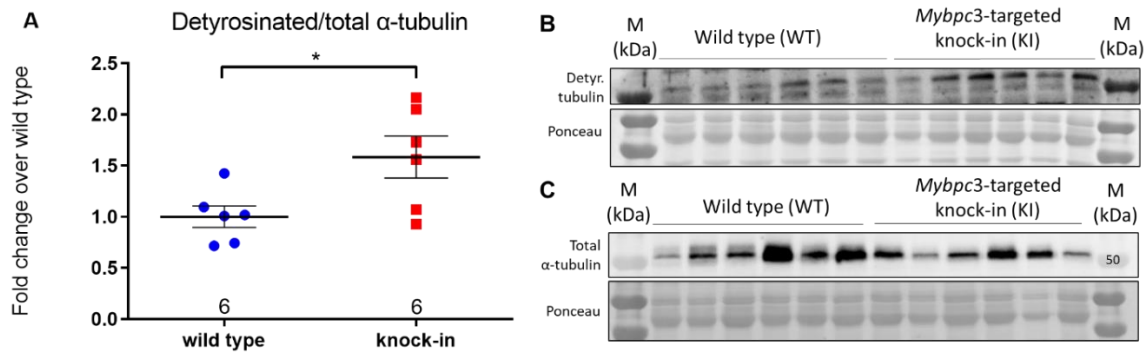


Figure 10: Protein levels of detyrosinated α -tubulin in wild-type (WT) and *Mybpc3*-targeted knock-in (KI) mice. (A) Ratio of detyrosinated α -tubulin to total α -tubulin in wild type and HCM model mice (n=6). **(B)** Representative Western Blot analysis with samples of WT and KI mice. Antibody staining for detyrosinated α -tubulin (Expected molecular weight: 52 kDa; n=6). **(C)** Representative Western Blot analysis with samples of WT and KI mice. Antibody staining for total α -tubulin (Expected molecular weight: 52 kDa; n=6). Ponceau as loading control. M = molecular weight marker. Data are expressed as mean \pm SEM. *p<0.05 (unpaired Student's t-test).

Detyrosinated α -tubulin levels were higher in KI mice than in WT (Figure 10, A and B). Analysis of total α -tubulin levels showed no significant differences between groups (data not shown). The detyrosinated/total α -tubulin ratio was 1.5-fold higher in KI than in WT mice (see Figure 10, A).

3.3. Investigation of detyrosinated and tyrosinated α -tubulin after tubulin modifications

The next aim of the study was to evaluate detyrosinated and tyrosinated tubulin protein levels in AMCMs after microtubule-modifying treatments. AMCMs were isolated from WT mice and treated with either 10 μ M paclitaxel or 10 μ M parthenolide for 2 hours to promote detyrosination or tyrosination of tubulin, respectively. As control, a third group of AMCMs was cultivated with DMSO, the solvent for both substances. Protein quantities were evaluated by Western Blot analysis and normalized to DMSO AMCMs. Ponceau and α -actinin stainings were used as loading controls (such as in Figure 6, C).

Treatment with paclitaxel induced a 5-fold increase in detyrosinated α -tubulin levels when compared to control. Parthenolide treatment did not have any effect on tubulin detyrosination (see Figure 11, A).

In a further batch of AMCMs changes of tyrosinated α -tubulin after treatment with paclitaxel (10 μ M) and parthenolide (10 μ M) were evaluated. The level of tyrosinated α -tubulin was 0.7-fold lower and 1.6-fold higher with paclitaxel and parthenolide treatment than DMSO-treated cardiomyocytes, respectively (see Figure 11, B).

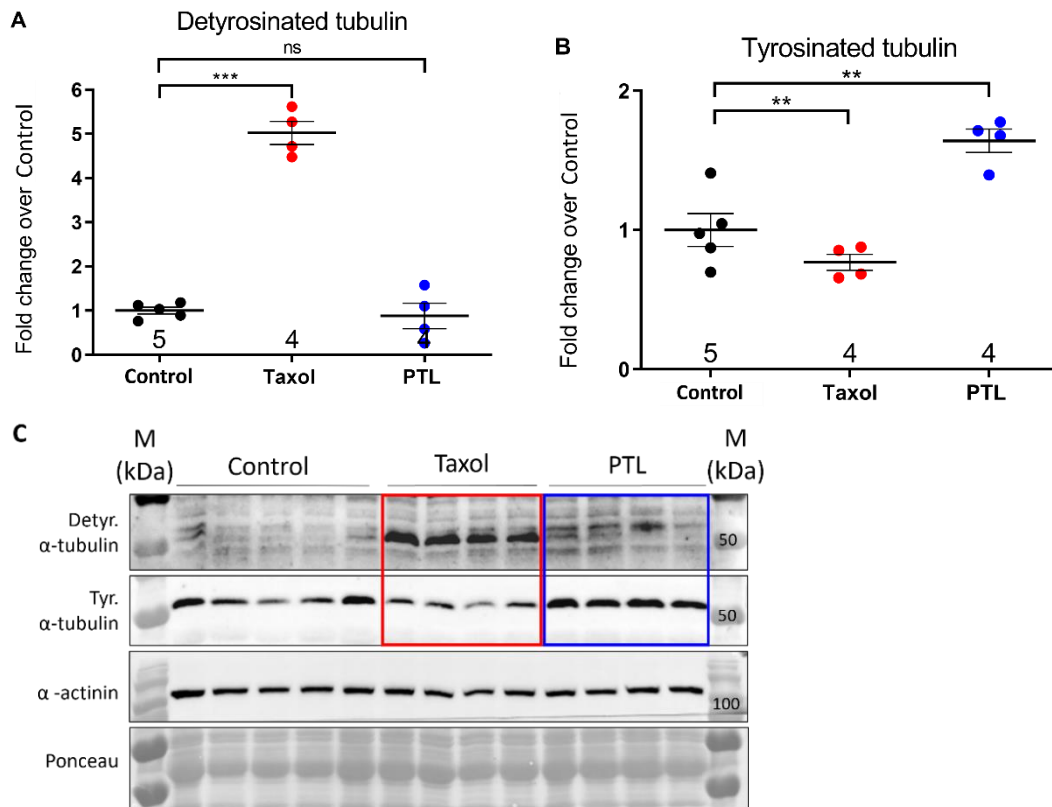


Figure 11: Protein levels of detyrosinated and tyrosinated α -tubulin after treatment with paclitaxel and parthenolide. (A) Quantification of detyrosinated α -tubulin levels in AMCMs harvested from a wild-type mouse at baseline after DMSO treatment (Control) and after treatment with 10 μ M paclitaxel (Taxol) or 10 μ M parthenolide (PTL) for 2 hours; n (control) = 5; n (Taxol; PTL) = 4. (B) Quantification of tyrosinated α -tubulin levels in AMCMs at baseline (untreated) and after treatment with 10 μ M paclitaxel (Taxol) or 10 μ M parthenolide (PTL) for 4 hours; n (untreated)= 5; n (Taxol; PTL) = 4. (C) Representative Western Blot analysis with protein lysates from AMCMs at baseline and after treatments (Taxol and PTL). Target proteins: detyrosinated α -tubulin and tyrosinated α -tubulin (both with expected molecular weight: 52 kDa); α -actinin (Expected molecular weight: 103 kDa) and Ponceau as loading control. M= molecular weight marker. Data are expressed as mean \pm SEM. $p^{**}<0.01$; $p^{***}<0.001$ vs. untreated (unpaired Student's t-test).

To assess whether changes in detyrosinated and tyrosinated α -tubulin protein level after microtubule modification could also be visualized in murine cardiomyocytes by immunofluorescence analysis, AMCMs were isolated from WT mice, treated with either DMSO, paclitaxel (10 μ M) or parthenolide (10 μ M), and then stained with primary antibodies which targeted the detyrosinated, tyrosinated or total form of α -tubulin. For improved visualization immunofluorescence was extended with antibodies targeting a sarcomeric protein, in this case α -actinin and a nuclear stain with DRAQ5™ (see Figure 12).

Untreated AMCMs displayed few scattered fluorescence signals with stronger α -tubulin detyrosination signal around the nucleus.

Treatment with paclitaxel resulted in an accumulation of detyrosinated α -tubulin with the formation of fluorescent conglomerates and overall increase in fluorescent intensity in visual comparison to control.

Two hours of parthenolide treatment appeared to result in a diminution of detyrosinated α -tubulin intensity throughout the myocyte, except for a constant signal around the nucleus (see Figure 12, last row).

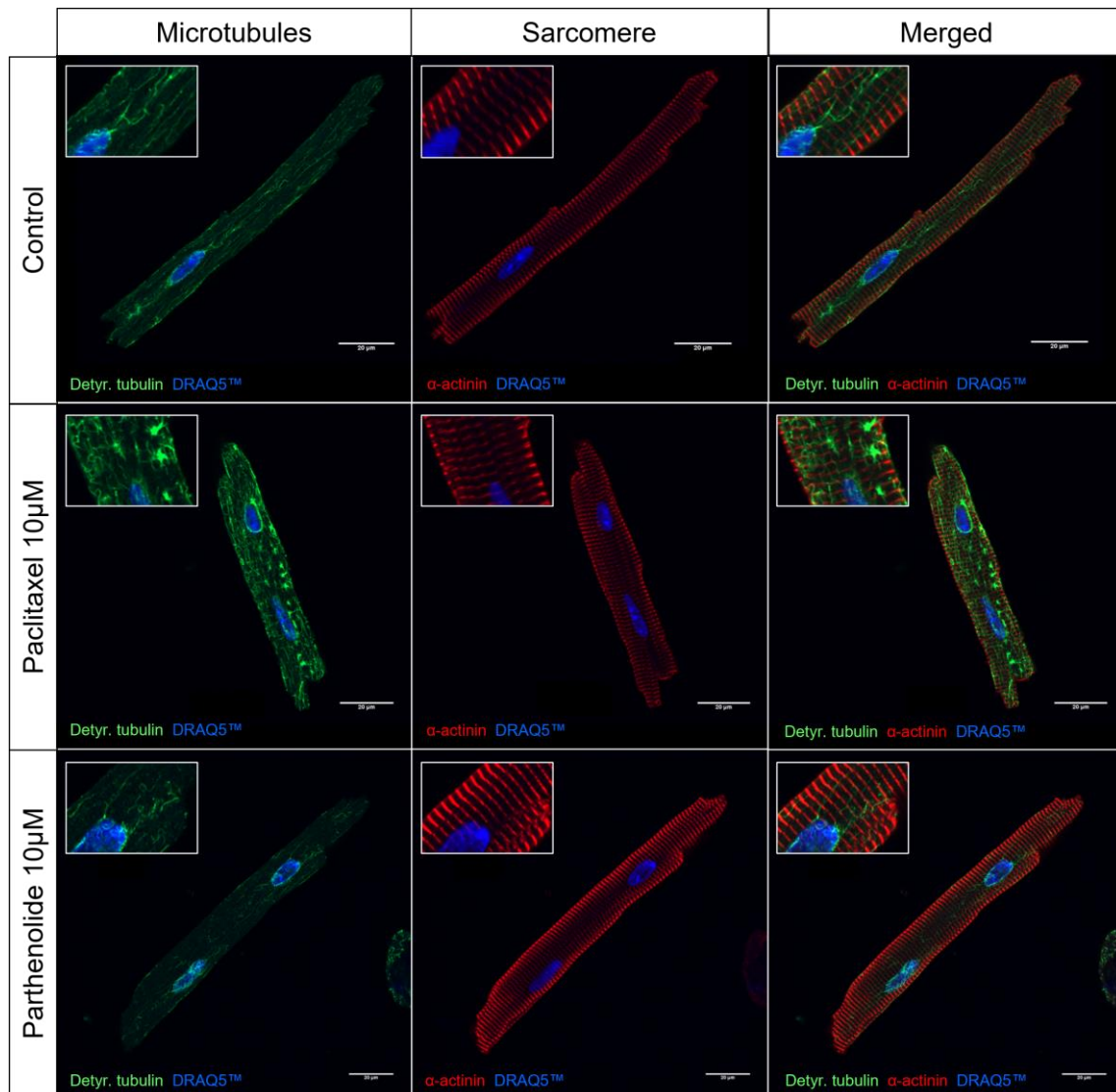


Figure 12: Immunofluorescence visualization of detyrosinated tubulin in treated AMCMs. Representative pictures of AMCMs isolated from WT mice DMSO (Control), paclitaxel (10 μ M) or parthenolide (10 μ M) for 2 hours under cell culture conditions (37 $^{\circ}$ C, 21% O₂, 2% CO₂, humidity > 90%). Immunofluorescence staining for detyrosinated tubulin (green), α -actinin (red) and DRAQ5 stain for nuclear visibility (blue). Pictures in the left column show microtubule staining, in the middle column the sarcomeric staining and the in right column a merged image. Scale: 20 μ m.

Next, the influence of microtubule modifying treatments on tyrosinated α -tubulin protein levels was investigated (Figure 13).

In the DMSO-treated AMCM, we see a widespread and evenly dispersed network of tyrosinated α -tubulin intensity throughout the cell, again with an enhancement of fluorescence intensity around the nucleus.

Treatment with paclitaxel for two hours resulted in a reduction of tyrosinated α -tubulin intensity when compared to control conditions, leaving behind a consistent area around the nucleus.

After parthenolide treatment tyrosinated α -tubulin intensity appeared slightly higher within the entire AMCM. No accumulation or formation of signal conglomerates was visible after treatments.

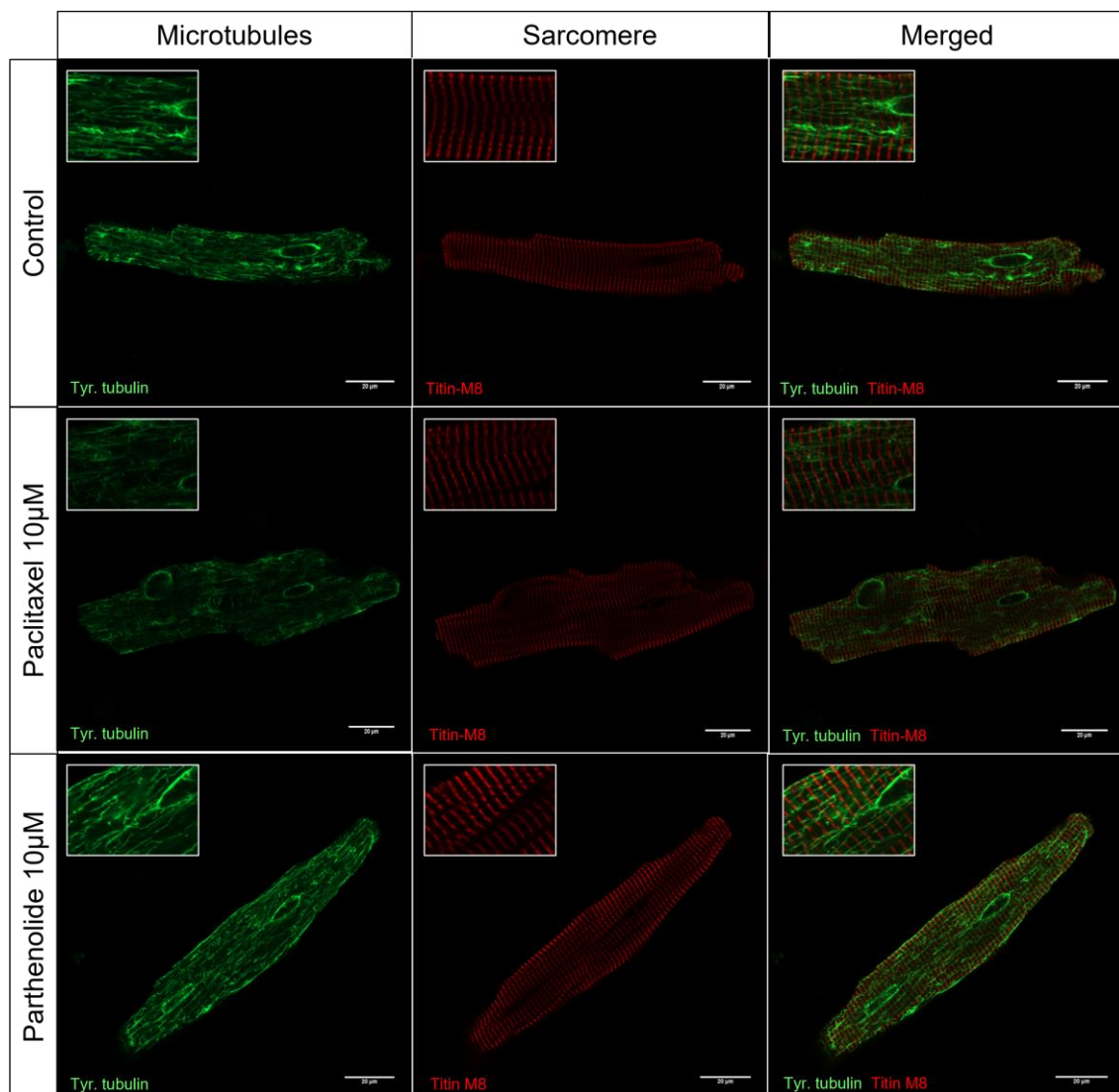


Figure 13: Immunofluorescence visualization of tyrosinated α -tubulin in treated AMCMs. Representative pictures of AMCMs isolated from WT mice treated with DMSO (control), paclitaxel (10 μ M) or parthenolide (10 μ M) for 2 hours under cell culture conditions (37 $^{\circ}$ C, 21% O₂, 2% CO₂, humidity > 90%). Immunofluorescence staining for tyrosinated α -tubulin (green) and Titin M-8 (red). Scale: 20 μ m.

Next the influence of paclitaxel and parthenolide on total α -tubulin was investigated. Immunofluorescence analysis was performed with a primary antibody targeting total α -tubulin. For sarcomere staining an antibody specific to cMyBP-C was used and nuclear stain with DRAQ5™ was added (see Figure 14).

Under control conditions a network of total α -tubulin was visible, evenly dispersed throughout the cardiomyocyte with an area of intensified signal around the nucleus.

Both paclitaxel and parthenolide treatments both seem to induce a similar slight intensification in total α -tubulin signal or dispersion when compared to the DMSO control.

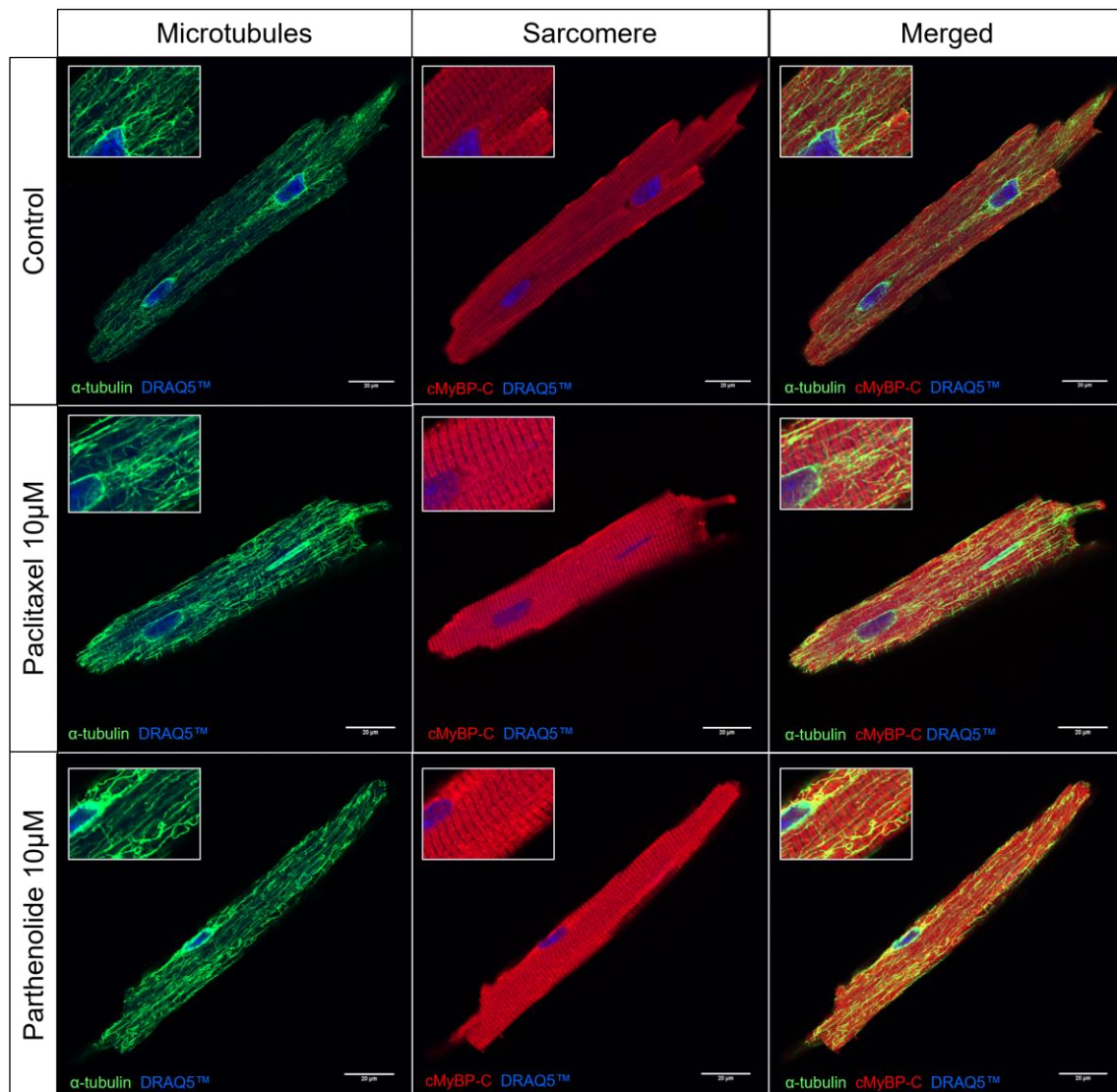


Figure 14: Immunofluorescence visualization of total α -tubulin in treated AMCMs. Representative pictures of AMCMs isolated from WT mice treated with DMSO (control), paclitaxel (10 μ M) or parthenolide (10 μ M) for 2 hours under cell culture conditions (37 °C, 21% O₂, 2% CO₂, humidity > 90%). Immunofluorescence staining for total α -tubulin (green), cMyBP-C (red) and DRAQ5 stain for the nucleus. Scale: 20 μ m.

3.4. Evaluation of protein-protein proximity

A further aim of the study was to investigate whether cMyBP-C interacts with the microtubule network. This was accomplished by using the proximity ligation assay (PLA) on isolated AMCMs, a technique to detect protein-protein proximity. It allows a sensitive and specific detection of protein complexes and hints towards individual interactions, while not providing a direct proof of interaction but rather a close proximity, as PLA signal is generated at target distances under 40 nm (Alam et al. 2018). For this method to provide credible findings, a variety of controls were established.

PLA was performed according to manufacturer protocol with slight adaptations for this cause (see methods). First, the feasibility and reliability of the method itself was tested in AMCMs. Therefore, a pair of primary antibodies targeting two proteins with known interaction, in this study total α -tubulin and desmin, was used (Salomon et al. 2022). As protein interaction under microtubule-modifying conditions was a further aim of this study this positive control was performed on AMCMs after treatment with either paclitaxel (10 μ M) or parthenolide (10 μ M) or DMSO as control.

Results show that PLA worked in AMCMs in DMSO-treated as well as after microtubule-modifying conditions, as red PLA signals for desmin and α -tubulin were generated in all experiments (see Figure 15). For improved visualization and to assure that PLA signals were mainly within the cell PLA was followed by immunofluorescence staining of the sarcomere and the nucleus. In this approach a primary antibody targeting cMyBP-C and DRAQ5™ were used.

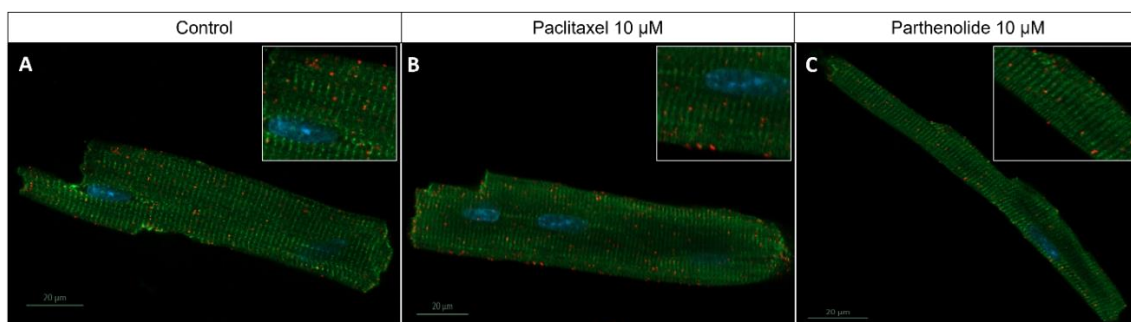


Figure 15: Positive control for Proximity Ligation Assay (PLA) for total α -tubulin and desmin. Shown are representative AMCMs isolated from WT mice and treated for 2 hours under cell culture conditions (37 °C, 21% O₂, 2% CO₂, humidity > 90%) with either DMSO (**A**), paclitaxel (10 μ M, **B**) or parthenolide (10 μ M, **C**). PLA signals (red) indicate proximity of proteins of interest. Image (A) shows a representative AMCM at control conditions, the cardiomyocyte in (**B**) was treated with 10 μ M paclitaxel and image (**C**) depicts an AMCM after treatment with parthenolide. PLA procedure was followed by immunofluorescence staining of cMyBP-C (green) and a DRAQ5 staining of the nucleus for visualization.

After validation of PLA in treated AMCMs the specificity of the method was tested. Therefore, several controls were tested during experiments. For the PLA to generate fluorescent product target proteins should be in close proximity, and specific primary antibodies targeting those proteins are required (for details see Methods). Negative controls were designed varying those two requirements. First, PLA was performed on WT AMCMs without primary antibodies. The corresponding experiment was performed according to the protocol and followed by an immunofluorescence stain for α -actinin. Excluding primary antibodies as targets for the PLA reaction led to no PLA red signal (see Figure 16, A).

In a different batch of AMCMs, the experiment was performed only using a single primary antibody, in our case an antibody targeting cMyBP-C. This produced sporadic, off-target PLA signals (see Figure 16, B).

An additional way to prove the procedures specificity was to perform the procedure according to protocol, including both primary antibodies, but on cells not expressing target proteins. Therefore, PLA was performed using isolated AMCMs from *Mybpc3*-targeted-KO-mice, which do not express any cMyBP-C (Carrier et al. 2004). For this control primary antibodies targeting cMyBP-C and microtubule-associated protein light chain 3 (LC3) were used, as the MYBPC3-sequence contains a putative LC3-interacting region (LIR) and interaction of these two proteins was shown in previous publications from our working group (see MD thesis by Marc von See, 2021). In the absence of one target protein the PLA generated no relevant amounts of fluorescent reaction product (see Figure 16, C). To assure that the method itself worked in *Mybpc3*-targeted-KO-AMCMs one more PLA was performed with primary antibodies targeting total α -tubulin and LC3, another known protein interaction (Mann and Hammarback 1994). This reaction produced lots of fluorescent PLA reaction product (see Figure 16, D).

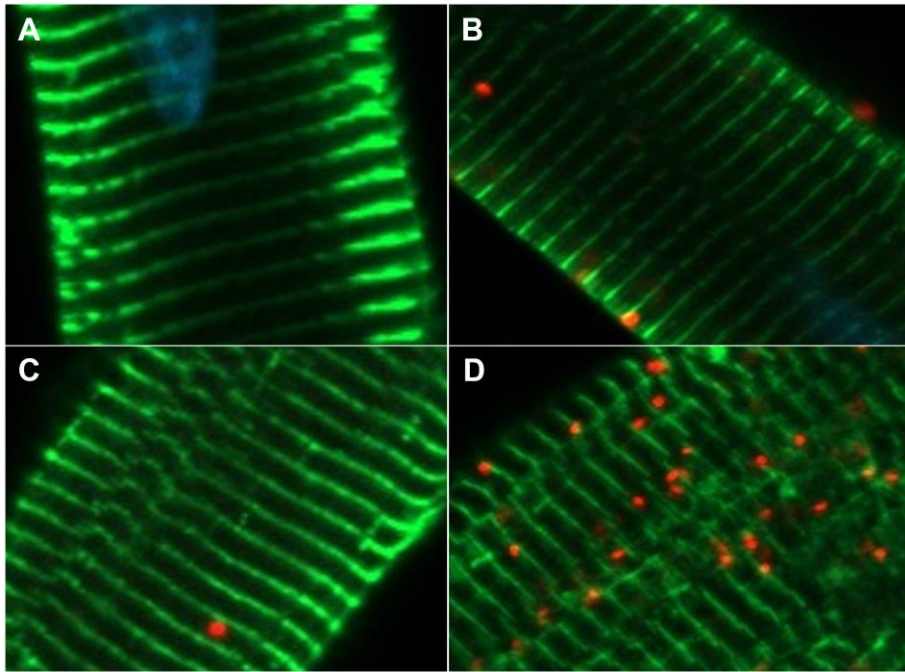


Figure 16: Negative and positive controls for Proximity Ligation Assay (PLA). Images (A) and (B) showed AMCMs isolated from a WT mouse. Cardiomyocytes in (C) and (D) were isolated from *Mybpc3*-targeted-KO-mice. PLA was performed on all depicted cells according to protocol. (A) shows results after no addition of primary antibodies, (B) after addition of only a single primary antibody (targeting cMyBP-C). In (C) PLA was performed with primary antibodies targeting LC3 and cMyBP-C. In (D) primary antibodies targeting LC3 and total α -tubulin were added. PLA was followed by immunofluorescence with an antibody staining α -actinin (green) in the sarcomere and DAPI (blue) for nuclear visualization.

As a final proof of concept PLA was performed on WT AMCMs with primary antibodies targeting two proteins in different cellular compartments and without known interaction. Used primary antibodies targeted lamin A/C, as part of the nuclear membrane and connexin 43, a member of the gap junction protein family located in the cell membrane. Before usage in PLA both antibodies were validated by immunofluorescence in isolated WT AMCMs. Both antibodies produced immunofluorescence signal according to the expected protein location (see Figure 17, B - C).

The PLA performed on isolated WT AMCMs with primary antibodies targeting connexin-43 and lamin A/C produced no fluorescent PLA signal (Figure 17), confirming their absence of proximity.

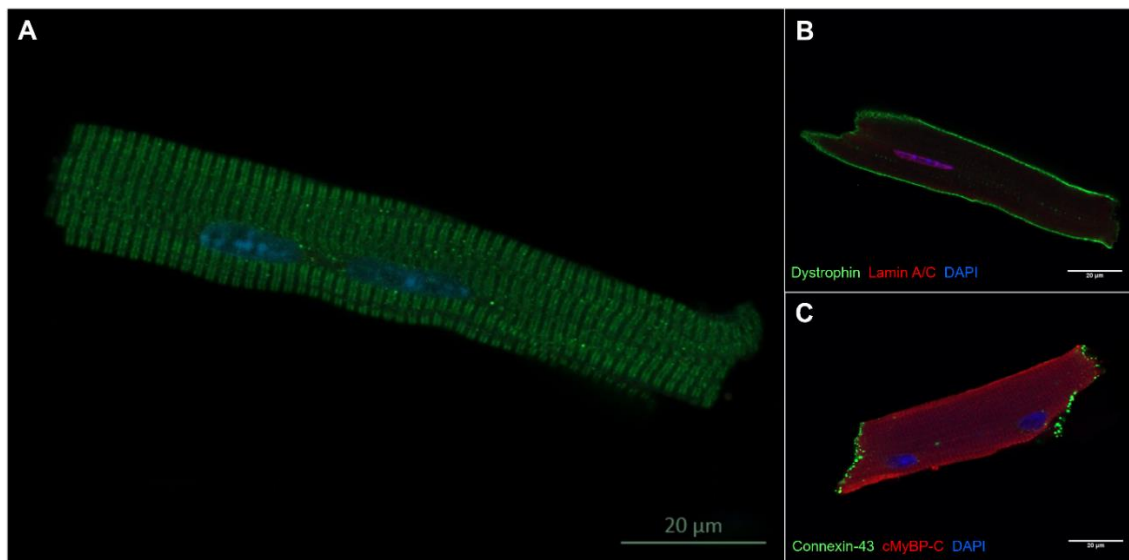


Figure 17: Negative Control for Proximity Ligation Assay (2). Shown in **(A)** to **(C)** are AMCMs harvested from wild-type mice. In **(A)** proximity ligation assay (PLA) was performed with primary antibodies targeting lamin A/C and connexin-43. PLA was followed by immunofluorescence staining of cMyBP-C (green) and DAPI (blue) for the nucleus. Image **(B)** shows immunofluorescence staining for lamin A/C (red), dystrophin (green) and the nucleus (DRAQ5). In **(C)** immunofluorescence was performed with primary antibodies targeting connexin 43 (green), cMyBP-C (red) and DRAQ5 (blue) for nuclear visibility. Scale: 20 μm .

3.4.1. Proximity of total α -tubulin and cMyBP-C

After establishing the PLA method and controls to be performed on AMCMs, the interaction of total α -tubulin and cMyBP-C was investigated. AMCMs were isolated from WT mice and treated with 10 μM paclitaxel, or 10 μM parthenolide or DMSO as a control. After tubulin modification for 2 hours PLA was performed with primary antibodies specific for total α -tubulin and cMyBP-C. The procedure was followed by an immunofluorescence staining for α -actinin and a nuclear DRAQ5TM-staining (see Figure 18).

The representative images showed that cMyBP-C and α -tubulin give rise to a PLA signal. The number of PLA between cMyBP-C and α -tubulin increased with paclitaxel, but not with parthenolide (see Figure 18).

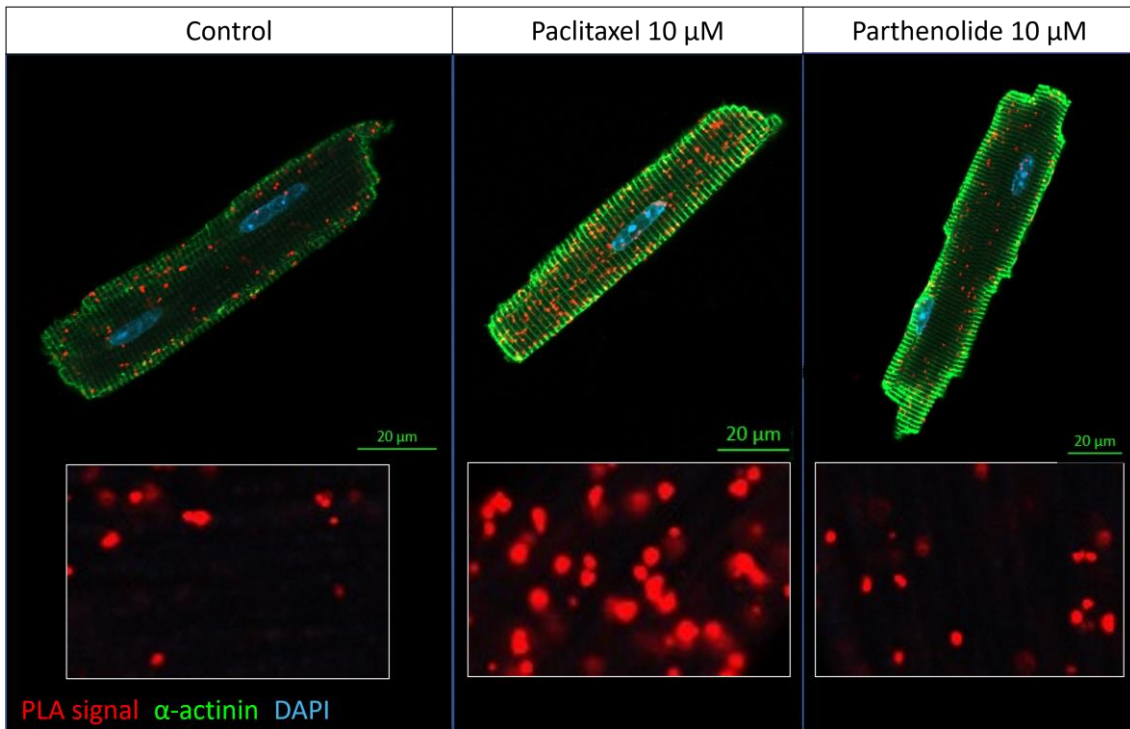


Figure 18: Proximity Ligation Assay analysis for total α -tubulin and cMyBP-C. Depicted are AMCMs isolated from WT mice either after DMSO-treatment (Control, left), treated with paclitaxel (10 μ M, middle) or parthenolide (10 μ M, right). Red signals within cells visualize the PLA product; boxes in the lower part of the picture show a representative magnification of cells above. PLA was followed by immunofluorescence staining of α -actinin (green) and the nucleus (DRAQ5, blue.) Scale: 20 μ m.

Quantification of PLA signal was performed according to protocol (see 2.10.). Under basal conditions the PLA produced a basal level of fluorescent reaction product.

After paclitaxel treatment experiment quantification showed a 1.4-fold increase in the reaction product when compared to control.

Parthenolide treatment did not lead to significant changes in PLA signal when compared to control (see Figure 19). These data suggest a close proximity between cMyBP-C and α -tubulin, which is higher in the presence of the stabilizing microtubule agent paclitaxel.

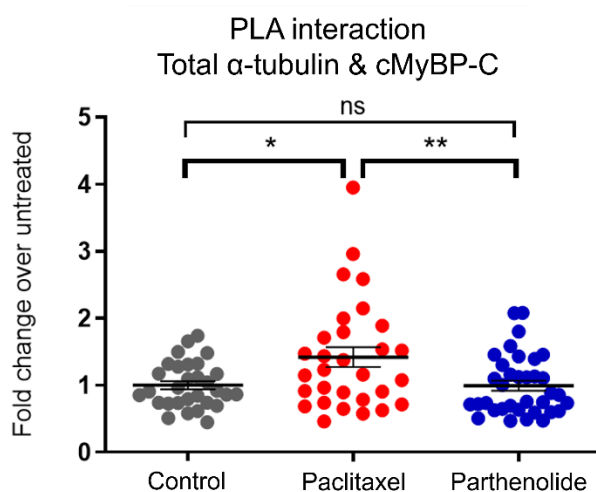


Figure 19: Quantification of proximity ligation assay product for total α -tubulin and cMyBP-C in basal conditions and after treatments. PLA signals were quantified in AMCMs isolated from WT mice after DMSO-treatment (control, n=30) and after tubulin modifications with either paclitaxel (10 μ M, n=30) or parthenolide (10 μ M, n=35) for two hours. Data are expressed as mean \pm SEM. *p<0.05 and p**<0.01 (unpaired t-test).

3.4.2. Proximity of detyrosinated α -tubulin and cMyBP-C

In the following approach interactions of cMyBP-C and detyrosinated α -tubulin was investigated. AMCMs were isolated from WT mice and treated with either 10 μ M paclitaxel, 10 μ M parthenolide or DMSO (control) according to protocol. PLA was performed with specific antibodies that targeted the detyrosinated form of α -tubulin and cMyBP-C. Procedure was followed by immunofluorescence staining with an α -actinin antibody and DRAQ5TM staining (see Figure 20). After PTL treatment nuclear elongation was observed in some cardiomyocytes (see Figure 20, right picture).

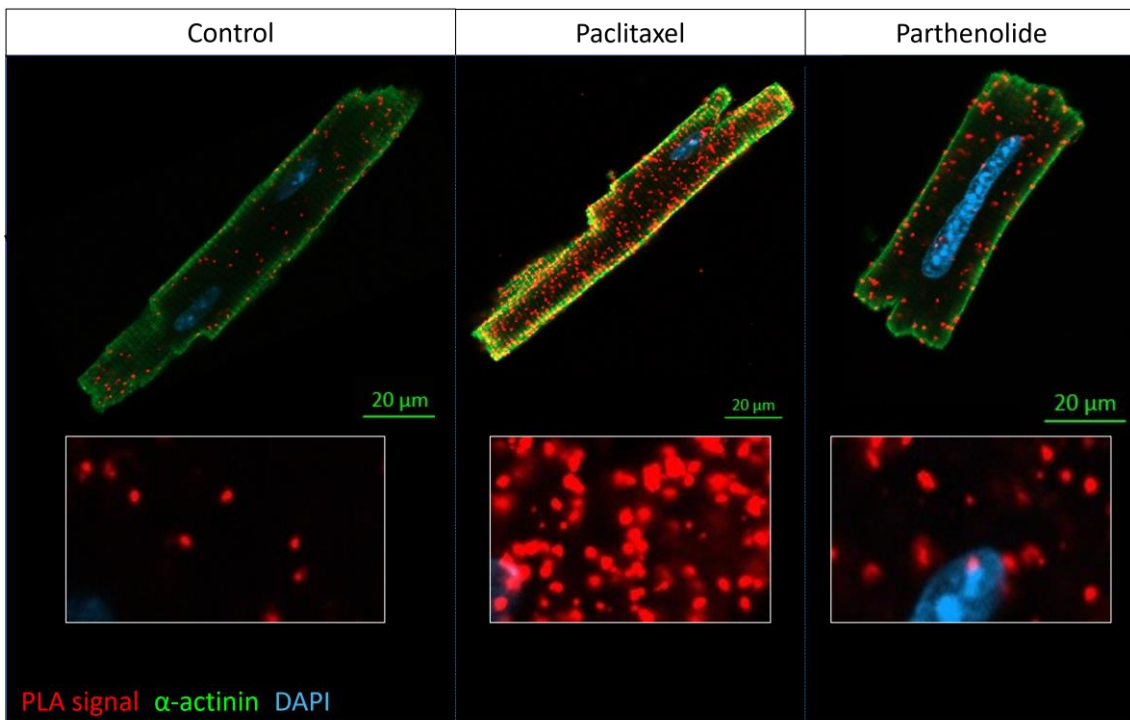


Figure 20: Proximity Ligation Assay analysis for detyrosinated α -tubulin and cMyBP-C. Depicted are AMCMs isolated from WT mice either after treatment with DMSO (Control, left), paclitaxel (10 μ M, middle) or parthenolide (10 μ M, right). Red signals within cells visualize the PLA product; boxes in the lower part show a representative magnification of cells above. PLA was followed by immunofluorescence staining of α -actinin (green) and the nucleus (DRAQ5, blue.) Scale: 20 μ m.

Under basal conditions PLA produced a level of fluorescent PLA product which was used as a normalization reference for quantification. Treatment with paclitaxel resulted in a more than 3-fold increase in the PLA product when compared to control (see Figure 21). This suggest that the stabilized, detyrosinated microtubules are in close proximity with cMyBP-C. Parthenolide treatment did not affect this proximity.

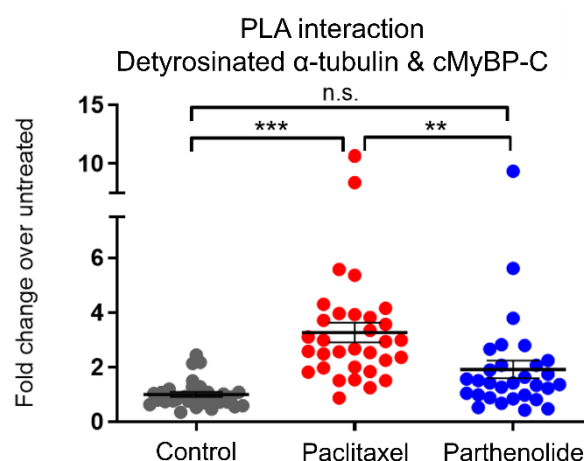


Figure 21: Quantification of proximity ligation assay product for detyrosinated α -tubulin and cMyBP-C in basal conditions and after treatments. PLA signals were quantified in AMCS isolated from WT mice after DMSO-treatment (control, n=30) and after microtubule modifications with either paclitaxel (10 μ M, n=32) or parthenolide (10 μ M, n=30) for two hours. Data are expressed as mean \pm SEM. $p^{**}<0.01$ and $***p<0.001$ vs. untreated (unpaired t-test).

4 Discussion

Cardiac myosin-binding protein C (cMyBP-C), a sarcomeric protein encoded by the *Mybpc3* gene was first discovered in 1973 (Offer et al. 1973). Since then, genetic variants in the *MYBPC3* gene were shown to be amongst the leading causes of inherited HCM (Schlossarek, Mearini et al. 2011). Current therapy mainly focuses on relief of symptoms while systematic causal therapy approaches remain missing (Ommen et al. 2020).

In recent years the microtubule network has been identified to play a relevant role in the pathophysiology of HCM. Increased detyrosination was shown to correlate with impaired myocardial function in rat models of HCM (Belmadani et al. 2002). This was consistent in septal myectomies from HCM patients (Robison et al. 2016). In this study we were able to confirm these findings within a homozygous *Mybpc3*-targeted knock-in mouse model, expressing a HCM typical phenotype (Vignier et al. 2009). To achieve this, specific antibodies targeting different posttranslational modifications of α -tubulin and cMyBP-C were successfully validated for Western Blot, immunofluorescence and proximity ligation assay in a first step.

With the help of Western Blot analysis, we were able to confirm generally elevated protein levels of detyrosinated α -tubulin in myocardial tissue samples from HCM patients and within our homozygous *Mybpc3*-targeted knock-in mouse model (see 3.2.).

A further approach was to modify the tyrosination state of microtubules within isolated AMCMs. Treatment with paclitaxel (Taxol®), a microtubule-stabilizing drug used in chemotherapy, induced a preponderance of detyrosinated α -tubulin in isolated cardiomyocytes, while a treatment with parthenolide, a sesquiterpene lactone known to inhibit the activity of the TCP, caused excessive detection of tyrosinated α -tubulin in the cardiomyocytes. This was shown both quantitatively in Western Blot and visually in immunofluorescence analysis (see 3.3.).

One mechanism suggested to lead to an impaired myocardial function in diseased hearts is an increased cytoskeletal stiffness due to an abundance of detyrosinated microtubules. In this model stabilized microtubules anchored on sarcomeric proteins, such as desmin, which acted like compression-bearing struts (Robison et al. 2016). However, the link between the frequent genetic variants (such as in the *MYBPC3* gene) found in HCM patients and the so far discovered molecular alterations remains unclear.

We proposed, following the idea of a stabilized microtubule network anchoring to sarcomeric proteins, that cMyBP-C can be a further anchor protein for especially the detyrosinated and therefore stabilized α -tubulin subpopulation. By PLA we evaluated the

protein-protein proximity between cMyBP-C and total α -tubulin, as well as the detyrosinated subpopulation, both at baseline and after microtubule-modifying treatments. We were able to provide evidence of a close proximity between total α -tubulin and cMyBP-C in basal conditions (see 3.4.2.). Addition of tubulin modifying drugs (paclitaxel and parthenolide) resulted in a change of PLA signal, where a significant increase in signal was detected after paclitaxel treatment but not after parthenolide. To specify whether the change in proximity after treatment resulted due to an accumulation of a specific subpopulation of α -tubulin, we evaluated proximity between detyrosinated α -tubulin and cMyBP-C (see 3.4.3). Here we could show a significant, more than 3-fold increase in PLA signal after paclitaxel treatment while parthenolide treatment did not lead to significant changes in signal. This suggests that the change in PLA signal (seen in 3.4.2.) is likely caused by a resulting stabilization of the polymerized microtubule network with abundance of the detyrosinated subpopulation after paclitaxel treatment with a following intensified interaction of sarcomeric and microtubular structures. The evaluation of protein proximity between tyrosinated α -tubulin and cMyBP-C was a further subject of interest, however due to a lack of primary antibody alternatives and a resulting mismatch of primary and secondary antibody during PLA procedure we were not able to further investigate the effects of microtubule-modifying drugs regarding the protein proximity of the pair. The data presented in this study confirm the close proximity of cMyBP-C and α -tubulin with a high affinity for the detyrosinated and therefore stabilized state. This supports the idea of cMyBP-C acting as a sarcomeric anchor for the microtubule network and underlines the importance in pathophysiology of HCM as stabilized, predominantly detyrosinated microtubules were shown to lead to suppressed contractile velocity and increased myocardial stiffness (Kreitzer et al. 1999, Robison et al. 2016).

In summary, the major findings of this study were the following:

- Detyrosinated microtubules accumulate in both septal myectomy from HCM patients and in homozygous *Mybpc3*-targeted knock-in mice, presenting with a typical HCM phenotype.
- Protein levels of detyrosinated and tyrosinated α -tubulin increased with the microtubule-modifying agents paclitaxel and parthenolide in isolated AMCMs, respectively.
- cMyBP-C and total α -tubulin are in close proximity suggesting an interaction between the two proteins (in vitro).
- Pharmacological induction of α -tubulin detyrosination results in an intensified microtubule-sarcomere proximity, at least between cMyBP-C and α -tubulin or detyrosinated α -tubulin.

4.1. Quantity of detyrosinated α -tubulin in HCM patients and mice

The microtubule network, consisting of heterodimers of α - and β -tubulin, contributes to a variety of processes in cellular homeostasis. This highly dynamic network can appear in a more condensed state, when diseased, leading to increased myocardial stiffness and overall impaired cardiac function as shown in a murine myoblast model (Kerr et al. 2015). With our own HCM mouse model, carrying a point mutation within the *Mybpc3* gene leading to the phenotypical expression of HCM, we hypothesized that along with findings in HCM patients and other animal models of diseased heart, there is an increased amount of detyrosinated α -tubulin. We were able to prove this hypothesis via Western Blot analysis with antibodies targeting detyrosinated α -tubulin. These findings verify this specific disease model for further investigation on pathogenesis of HCM on the way to finding curative therapy approach.

4.2. Detyrosinated α -tubulin and modifications

Microtubular function and appearance is determined by a multitude of factors which have been proposed over the years. Amongst them posttranslational modifications have emerged as possible regulators of properties and assembly resulting in a variety of microtubule isotypes (Janke and Bulinski 2011). The reversible attachment and removal of the C-terminal tyrosine residue on α -tubulin, leading to a tyrosinated or detyrosinated microtubule, is mediated by enzymatic processes. The process of tyrosination is

catalyzed by a long-known TTL, which works on soluble α -/ β -tubulin heterodimers (Gundersen et al. 1987). The reverse process, the detyrosination of α -tubulin, is mediated by a more recently discovered tubulin TCP. This TCP is a complex of vasohibin-1 (VASH1) or the vasohibin-2 (VASH2) and their chaperone, the vasohibin binding protein (SVBP), which was shown to exhibit a specific carboxypeptidase activity on C-terminal tyrosine in microtubules of murine brain tissue (Aillaud et al. 2017). While the early experiments were conducted on murine brain tissue various vasohibins are abundant in multiple organ systems such as cardiac or renal tissue (Nimmagadda et al. 2007). It was shown that the complex of VASH1 and SVBP is predominantly responsible for the TCP function in cardiomyocytes. Furthermore, Inhibition of VASH1 or the activation of the TTL resulted in an increase of relaxation velocity, a major phenotypical impairment found in HCM-related HF (Chen et al. 2020).

In this study we showed and confirmed the effects of paclitaxel (Taxol®) and parthenolide on the detyrosination/re-tyrosination cycle of microtubules of isolated AMCMs. While Western Blot analysis showed a 5-fold increase in detyrosinated α -tubulin after paclitaxel treatment (see Fig. 11), the corresponding immunofluorescence analysis visualized this effect with an overall increase in IF signal and multiple sites of signal accumulation along the sarcomere and in the perinuclear region, respectively ncMTOCs (see Fig. 12). This accumulation of IF signal may occur due to an increased interaction of detyrosinated α -tubulin with components of the sarcomere, such as the known interaction with desmin (Robison et al. 2016), or novel anchoring proteins for the microtubule network such as cMyBP-C as we propose in this work. A further explanation for this phenomenon could be a damaging of the microtubule network during preparation and pharmacological treatment. Stress conditions, such as mechanical, osmotic or hypoxic, are shown to induce reorganization of the microtubule network and microtubule-mediated clustering of organelles, especially within the perinuclear region, while triggering nuclear remodeling as response to maintain structural integrity and adapt to environmental changes (Al-Mehdi et al. 2012, Nunes et al. 2013, Hoffman et al. 2020). While this might be an explanation of IF and PLA signal accumulation within the perinuclear region it does not explain the abundance of interaction throughout the entirety of the sarcomere sufficiently. Further, the consistency of accumulating microtubule signal throughout multiple approaches and the absence of it in the same batch but with varying primary antibodies make this unlikely. To achieve further prove of interaction between detyrosinated α -tubulin and in our case cMyBP-C additional *in vivo* analysis techniques

of protein-protein interaction are needed, such as BioID, a more recently developed biotin ligase mediated proximity-dependent labeling method (Roux et al. 2018).

Treatment with parthenolide on the other hand resulted in a 1.6-fold increase in tyrosinated α -tubulin in Western Blot analysis while visual effects of the treatment in immunofluorescence were not as noteworthy when compared to images of detyrosinated α -tubulin after paclitaxel treatment. The effect of parthenolide treatment on levels of detyrosinated α -tubulin was not significant, neither quantitatively in Western Blot analysis nor visually in immunofluorescence. This might have been increased with higher concentrations of parthenolide in the medium or longer exposure to the treatment itself, but to sustain comparability between the treated groups exposure time was kept equal. Higher concentrations of parthenolide on the other hand are described to create relevant off-target effects with regard to calcium handling and cell signaling cascades which make the chemical in higher concentrations rather unviable as a possible substance for reduction of detyrosination in therapy (Wen et al. 2002, Ghantous et al. 2013, Chen et al. 2018). Therefore, there remains need for other specific therapeutic approaches to inhibit the function of the TTL. A further incidental finding after PTL treatment was a nuclear enlargement. This effect might be explained with regard to the depolarizing effects of PTL on the microtubule network, leading to a more dynamic nuclear structure due to a lack of microtubular stabilization.

While targeting the activity of the TTL pharmacologically to induce depolymerization in cardiomyocytes appears to be complicated for now the more recent discovery of the TCP, responsible for the enzymatic removal of the C-terminal tyrosine residue, appears to be a promising target for future therapeutic approaches, either pharmacologically or via gene therapy.

4.3. Proximity Ligation Assay

The proximity ligation assay (PLA) method is a molecular biology technique used to detect protein-protein proximity, post-translational modifications, and protein localization. It allows for sensitive and specific detection of protein complexes and enables the visualization of individual interactions within complex biological systems. PLA is widely employed in various research areas, including cell biology, immunology, cancer research, and drug discovery, providing valuable insights into signaling pathways, protein dynamics, and disease mechanisms.

Proximity-dependent labeling allows to resolve nano-environments of target proteins in situ where prior, more traditional techniques, such as immunoprecipitation coupled with

mass spectrometry, had their limitations due to the need for high-quality antibodies and the insufficient detection in low-affinity or transient interactions (Roux et al. 2012, Kushner et al. 2022).

While the PLA method is a valuable tool, it also presents some challenges. It can be technically demanding and time-consuming, requiring optimization for each specific protein pair or target. False positives and background noise can occur, requiring careful experimental design and controls. In this study we used a variety of controls to confirm the method for the use in cardiomyocytes and minimize the probability and influence of a non-specific PLA product generation. As a positive control, to ensure the viability of the method in our study, primary antibodies targeting proteins with an already established interaction, in this case total α -tubulin and desmin were chosen (Salomon et al. 2022). We showed that PLA signals were created in control AMCMs and after treatment with paclitaxel and parthenolide. To provide certainty of the specificity of the method a variety of negative controls were initially established. The addition of no or only a single primary antibody, while performing the rest of the PLA according to protocol, led to no or sporadic PLA signal. Further, a pair of primary antibodies was used targeting a putative protein-protein interaction (cMyBP-C and LC3 since cMyBP-C contains a LC3-interacting region) but on cells lacking one of the specific targets, in our case AMCMs isolated from *Mybpc3*-KO-mice which, are described to express no cMyBP-C. After performing the PLA according to protocol no relevant amounts of reaction product were generated. For the final negative control, primary antibodies specific for lamin A/C and connexin 43 were used, two proteins that are located in different cellular compartments. The experiment resulted in no production of PLA signal. To guarantee the specificity of each PLA two negative controls, one without primary antibodies and a second with only a single primary antibody, were used in every approach. By summarizing the results of the various controls, we performed on the murine cardiomyocytes, we confirmed the PLA as a viable and specific method to investigate protein-protein proximity in cardiomyocytes isolated from adult mice, both under baseline conditions and after pharmacological treatment with paclitaxel and parthenolide.

A further obstacle was the interpretation of PLA results which can also be complex, as proximity does not necessarily indicate direct interaction. However, prior experiments in our workgroup using Co-immunoprecipitations, as a direct way to demonstrate protein-protein interaction, were not able to overcome procedural issues and finally not successful on isolated murine cardiomyocytes as the method relies on the principle that interactions must be preserved during cell lysis and purification of complexes. This

however can be challenging when interactions or proteins of interest easily lose integrity through purification or appear difficult to solubilize (Samavarchi-Tehrani et al. 2020).

After establishing the specificity of the PLA method in our model via various controls a further hindrance had to be addressed. A weakness of the PLA method lies in its limited capability for direct quantification of PLA products. PLA primarily provides qualitative information about the presence or absence of protein-protein interactions or modifications. While the number of PLA signals can provide a semi-quantitative indication of the relative abundance, it does not offer precise quantification. The intensity of PLA signals can be influenced by various factors, including antibody affinities, local protein concentrations, and experimental conditions, making it challenging to derive accurate quantitative measurements. While there are several tools designed to recognize and analyze a spherically shaped cell for PLA quantification provided by different software companies, such as ImageJ, CellProfiler and MATLAB, these programs struggle severely with the detection of rod-shaped, non-spherical cardiomyocytes. To generate quantitative data, we used the digital imaging analysis tool by the public domain software ImageJ with the “FIJI” image processing package and established a protocol with a semi-automatized detection of cellular area and PLA signal. During the process of detection, a visual control by the user is necessary to select the precise cell area and differentiate the PLA signal from the background. This step was needed due to the lack of an automatized cell area recognition and can make the results varying in between different users. To address this issue, in our study all data quantification was handled by the same user to mitigate the influence of inter-user variability. For further PLA analysis of cardiomyocytes in the future supplementary quantitative techniques or modifications, such as using digital automatized imaging analysis or incorporating standard curves, may be required for more precise quantification in PLA-based studies.

A final limitation of the PLA method might be the limited availability of suitable antibodies. PLA relies on the use of specific antibody pairs that recognize and bind to the target proteins of interest. However, not all proteins have well-characterized antibodies available, limiting the applicability of PLA for certain protein targets. This constraint can hinder researchers from investigating protein interactions or modifications that lack validated antibody pairs. Efforts to expand the repertoire of high-quality antibodies for

various proteins can help address this limitation and enhance the utility of PLA in a wider range of studies.

Despite the mentioned challenges, careful execution and validation can help to overcome these limitations and ensure reliable and meaningful results, making PLA a viable tool for the investigation of protein-protein interaction in cardiomyocytes.

4.4. Co-localization of α -tubulin and cMyBP-C

One of the main novel findings of this study was the co-localization and assumed interaction of cMyBP-C and α -tubulin. Both total α -tubulin and the subfraction of detyrosinated α -tubulin were shown to interact with cMyBP-C at control conditions and after pharmacological treatment with paclitaxel or parthenolide. This can act as evidence to support the hypothesis of cMyBP-C acting as a further molecular anchor protein for the microtubule network in cardiomyocytes.

Along this hypothesis, keeping in mind that a stiff and to an increased degree detyrosinated microtubule network is suggested to be a pathomechanism in the development of HCM, we investigated whether increased detyrosination of α -tubulin induces more interaction between the microtubule network and cMyBP-C as a sarcomeric anchor protein. Treatment with paclitaxel resulted in an increase PLA signal between total α -tubulin and cMyBP-C, supposedly due to an over proportional increase of the detyrosinated α -tubulin subfraction. This effect was confirmed in the PLA analyzing the interaction of detyrosinated α -tubulin and cMyBP-C, where a significant, more than 3-fold, increased interaction was observed after paclitaxel treatment. This finding goes in line with the hypothesis that the abundance of detyrosinated α -tubulin in HCM patient-derived cardiac tissue enhances the interaction between the microtubule system and the sarcomere (Schuldt et al. 2021) This stronger interaction can be a key factor in the development of HCM, leading to major features observed in the disease, which are increased myocardial stiffness and diastolic dysfunction.

Whether the increased detyrosination of α -tubulin and therefore the putative interaction of the microtubule network with cMyBP-C is a direct result of the frequently disease-associated *MYBPC3* mutation remains uncertain. An explanation could be the induction of VASH1/SVBP-complex and/or increased TCP activity. A resulting change in protein conformation with the expression of new or altered binding sites, especially for detyrosinated α -tubulin can be possible as well. Today, we are still lacking data on this topic which making it an interesting subject for investigation in the further approach of understanding the role of microtubules and cMyBP-C in HCM.

5 Summary

The main scientific interests of our group for several years are genetics, pathophysiology and gene therapy of hypertrophic cardiomyopathy (HCM). HCM is an autosomal-dominant disorder characterized by cardiac hypertrophy and dysfunction caused by genetic variants in genes encoding sarcomeric components. Out of them, *MYBPC3*, encoding cardiac myosin-binding protein C (cMyBP-C), is the most frequently mutated one.

The group previously developed mouse models of HCM that exhibit low level (knock-in) of or no (knock-out) cMyBP-C and develop cardiomyopathy (Carrier et al. 2004, Vignier et al. 2009). Recent insights point to the importance of microtubule dynamics and α -tubulin posttranslational modifications (e.g. detyrosination) in cardiomyopathy (Kerr et al. 2015, Robison et al. 2016). Specifically, detyrosination of α -tubulin is associated with stable microtubules and cardiomyocyte stiffness. However, the interplay between components of the sarcomere and microtubules has not been evaluated in detail yet.

In this work we were interested to measure protein levels of detyrosinated α -tubulin in cardiac tissue derived from HCM patients and from *Mybpc3*-targeted knock-in mice, our HCM mouse model. Further the effects of pharmacological microtubule modulation were at interest. Finally, we investigated possible interactions between the microtubule network and cMyBP-C as a possible novel anchoring point of the microtubules within the sarcomere.

By using Western Blot analysis, we showed significantly elevated protein levels of detyrosinated α -tubulin in cardiac tissue derived from both human HCM and *Mybpc3*-targeted KI mice, while total α -tubulin protein level remained constant. Further, we established a protocol to induce detyrosination of α -tubulin in isolated AMCMs with paclitaxel, a microtubule-stabilizing drug used in chemotherapy. Via immunofluorescence we stained the microtubule network in AMCMs and visualized an accumulation of detyrosinated α -tubulin in paclitaxel-treated myocytes. Further we set up a model to investigate protein-protein proximity in isolated AMCMs using proximity ligation assay (PLA), which allows for sensitive and specific detection of potential protein complexes. Here we showed a close proximity between cMyBP-C and α -tubulin, especially in its detyrosinated state. Unfortunately, we were not able to include a PLA on the interaction of tyrosinated tubulin, a rat-derived antibody, and cMyBP-C due to a lack of corresponding PLA Probes for our tyrosinated tubulin antibody.

In summary we assume cMyBP-C to be a novel anchor protein for the microtubule network in the sarcomere of cardiomyocytes. Treatment with paclitaxel induced α -tubulin

detyrosination and increased PLA signal with cMyBP-C. The overall elevated protein levels of detyrosinated α -tubulin along with a potential increased interaction of condensed microtubules and the cMyBP-C anchor within the sarcomere could explain the increased myocardial stiffness and diastolic dysfunction observed in patients suffering from HCM.

Whether the increased detyrosination of α -tubulin and therefore interaction of microtubule network and cMyBP-C is a direct result of the frequently disease-associated *MYBPC3* genetic variants with an increase in TCP activity or a resulting change in protein conformation with the expression of new or altered binding sites, remains uncertain and should be subject to investigation with a further approach of understanding the role of microtubules and cMyBP-C in HCM in near future.

6 Zusammenfassung

Seit vielen Jahren widmet sich unsere Arbeitsgruppe der Erforschung von Genetik, Pathophysiologie und Gentherapie der hypertrophen Kardiomyopathie (HCM). Die HCM ist eine autosomal-dominant vererbte Erkrankung charakterisiert durch kardiale Hypertrophie und Dysfunktion, ausgelöst durch Mutationen in verschiedenen Genen, welche für die Expression diverser sarkomerischer Proteine verantwortlich sind. Unter ihnen ist das *MYBPC3*-Gen, welches für das kardiale Myosin-bindende Protein C (cMyBP-C) kodiert, am häufigsten von Mutationen betroffen (Carrier et al. 2015).

Der Arbeitsgruppe ist es gelungen Mausmodelle der HCM zu entwickeln, welche entweder vermindert (knock-in) oder kein (knock-out) cMyBP-C exprimieren und eine Kardiomyopathie entwickeln (Carrier et al. 2004, Vignier et al. 2009). Neuere Erkenntnisse weisen der Dynamik und den posttranslationalen Modifikationen der Mikrotubuli, vor allem der Detyrosinierung, eine relevante Rolle im Rahmen von Kardiomyopathien zu (Kerr et al. 2015, Robison et al. 2016). Vor allem die Detyrosinierung von α -Tubulin führt zu einer Stabilisierung der Mikrotubuli und führt zu myokardialer Versteifung. Bislang liegt jedoch noch keine detaillierte Untersuchung des Zusammenspiels von Bestandteilen des Sarkomers und den Mikrotubuli vor.

Ziel dieser Arbeit war die Bestimmung von detyrosiniertem α -Tubulin in Herzgewebe, welche von Patienten mit HCM oder *Mybpc3*-gezielten knock-in Mäusen, unserem HCM-Mausmodell, gewonnen wurden. Des Weiteren wurde der Einfluss auf Tyrosinierung nach Tubulin-modifizierender pharmakologischer Behandlung untersucht. Abschließend wurden mögliche Interaktionspunkte zwischen dem Mikrotubuli-Netzwerk and cMyBP-C, als möglicher neuer Ankerpunkt im Sarkomer, untersucht.

In dieser Arbeit konnten wir mittels Western Blot Analyse signifikant erhöhte Werte von detyrosiniertem α -Tubulin in Herzgewebe von HCM-Patienten und *Mybpc3*-gezielten knock-in Mäusen nachweisen, während die Menge an gesamtem α -Tubulin unverändert blieb. Zudem gelang die Etablierung eines Protokolls zur Induktion der Detyrosinierung von α -Tubulin in isolierten adulten Maus Kardiomyozyten (AMCM) mittels Paclitaxel, einer gegen Tubulin gerichteten Substanz, welche auch in der Chemotherapie Anwendung findet. Mit Hilfe von Immunfluoreszenz wurde das Mikrotubuli-Netzwerk in AMCMs gefärbt und so eine Akkumulation von detyrosiniertem α -Tubulin in Paclitaxel-behandelten Myozyten nachgewiesen. In einem weiteren Schritt etablierten wir ein Modell zur Untersuchung von Protein-Protein-Interaktionen in AMCMs mithilfe der Proximity Ligation Assay (PLA)-Methode, welche eine sensitive und spezifische Detektion von Proteinkomplexen sowie eine Visualisierung von individuellen Proteininteraktionen ermöglicht. Hier konnten wir eine bislang unbekannte Interaktion

zwischen cMyBP-C und Tubulin aufzeigen, bevorzugt in der detyrosinierten Form. Wir folgern entsprechend, dass cMyBP-C ein weiteres Ankerprotein für das Mikrotubuli-Netzwerk im Sarkomer von Kardiomyozyten sein kann. Behandlung mit Paclitaxel induzierte die Detyrosinierung und somit auch eine Interaktion von cMyBP-C und den Mikrotubuli. Der insgesamt erhöhte Proteingehalt an detyrosiniertem α -Tubulin gemeinsam mit einer vermehrten Interaktion von kondensierten Mikrotubuli und dem cMyBP-C-Anker können eine Erklärung für die erhöhte myokardiale Steifheit sein, welche in HCM-Patienten beobachtet wird.

Ob ein erhöhter Anteil an Detyrosination von α -Tubulin und damit eine vermehrte Interaktion zwischen Mikrotubuli-Netzwerk und cMyBP-C eine direkte Folge der häufig krankheitsassoziierten *MYBPC3*-Mutation mit einer Überregulation der Tubulin Carboxypeptidase (TCP)-Aktivität ist oder eher eine Veränderung der Proteinkonformation mit der Expression neuer oder veränderter Bindungsstellen, bleibt bis dato ungeklärt und bedarf in Zukunft weiterer Untersuchung mit dem Anspruch die Rolle der Mikrotubuli und cMyBP-C in HCM zu verstehen.

7 Literature

1. Aillaud, C., C. Bosc, L. Peris, A. Bosson, P. Heemeryck, J. Van Dijk, J. Le Friec, B. Boulan, F. Vossier, L. E. Sanman, S. Syed, N. Amara, Y. Coute, L. Lafanechere, E. Denarier, C. Delphin, L. Pelletier, S. Humbert, M. Bogyo, A. Andrieux, K. Rogowski and M. J. Moutin (2017). "Vasohibins/SVBP are tubulin carboxypeptidases (TCPs) that regulate neuron differentiation." *Science* **358**(6369): 1448-1453.
2. Akhmanova, A. and M. O. Steinmetz (2008). "Tracking the ends: a dynamic protein network controls the fate of microtubule tips." *Nat Rev Mol Cell Biol* **9**(4): 309-322.
3. Al-Mehdi, A. B., V. M. Pastukh, B. M. Swiger, D. J. Reed, M. R. Patel, G. C. Bardwell, V. V. Pastukh, M. F. Alexeyev and M. N. Gillespie (2012). "Perinuclear mitochondrial clustering creates an oxidant-rich nuclear domain required for hypoxia-induced transcription." *Sci Signal* **5**(231): ra47.
4. Arce, C. A., J. A. Rodriguez, H. S. Barra and R. Caputo (1975). "Incorporation of L-tyrosine, L-phenylalanine and L-3,4-dihydroxyphenylalanine as single units into rat brain tubulin." *Eur J Biochem* **59**(1): 145-149.
5. Authors/Task Force, m., P. M. Elliott, A. Anastasakis, M. A. Borger, M. Borggrefe, F. Cecchi, P. Charron, A. A. Hagege, A. Lafont, G. Limongelli, H. Mahrholdt, W. J. McKenna, J. Mogensen, P. Nihoyannopoulos, S. Nistri, P. G. Pieper, B. Pieske, C. Rapezzi, F. H. Rutten, C. Tillmanns and H. Watkins (2014). "2014 ESC Guidelines on diagnosis and management of hypertrophic cardiomyopathy: the Task Force for the Diagnosis and Management of Hypertrophic Cardiomyopathy of the European Society of Cardiology (ESC)." *Eur Heart J* **35**(39): 2733-2779.
6. Baas, P. W., A. N. Rao, A. J. Matamoros and L. Leo (2016). "Stability properties of neuronal microtubules." *Cytoskeleton (Hoboken)* **73**(9): 442-460.
7. Behrens-Gawlik, V., G. Mearini, C. Gedicke-Hornung, P. Richard and L. Carrier (2014). "MYBPC3 in hypertrophic cardiomyopathy: from mutation identification to RNA-based correction." *Pflugers Arch* **466**(2): 215-223.
8. Belmadani, S., C. Pous, R. Ventura-Clapier, R. Fischmeister and P. F. Mery (2002). "Post-translational modifications of cardiac tubulin during chronic heart failure in the rat." *Mol Cell Biochem* **237**(1-2): 39-46.
9. Caporizzo, M. A., C. Y. Chen and B. L. Prosser (2019). "Cardiac microtubules in health and heart disease." *Exp Biol Med (Maywood)* **244**(15): 1255-1272.
10. Carrier, L. (2021). "Targeting the population for gene therapy with MYBPC3." *J Mol Cell Cardiol* **150**: 101-108.
11. Carrier, L., G. Bonne, E. Barend, B. Yu, P. Richard, F. Niel, B. Hainque, C. Cruaud, F. Gary, S. Labeit, J. B. Bouhour, O. Dubourg, M. Desnos, A. A. Hagege, R. J. Trent, M. Komajda, M. Fiszman and K. Schwartz (1997). "Organization and sequence of human cardiac myosin binding protein C gene (MYBPC3) and identification of mutations predicted to produce truncated proteins in familial hypertrophic cardiomyopathy." *Circ Res* **80**(3): 427-434.
12. Carrier, L., R. Knoll, N. Vignier, D. I. Keller, P. Bausero, B. Prudhon, R. Isnard, M. L. Ambrosine, M. Fiszman, J. Ross, Jr., K. Schwartz and K. R. Chien (2004). "Asymmetric septal hypertrophy in heterozygous cMyBP-C null mice." *Cardiovasc Res* **63**(2): 293-304.
13. Carrier, L., G. Mearini, K. Stathopoulou and F. Cuello (2015). "Cardiac myosin-binding protein C (MYBPC3) in cardiac pathophysiology." *Gene* **573**(2): 188-197.
14. Chen, C. Y., M. A. Caporizzo, K. Bedi, A. Vite, A. I. Bogush, P. Robison, J. G. Heffler, A. K. Salomon, N. A. Kelly, A. Babu, M. P. Morley, K. B. Margulies and B. L. Prosser (2018). "Suppression

- of detyrosinated microtubules improves cardiomyocyte function in human heart failure." Nat Med **24**(8): 1225-1233.
15. Chen, C. Y., A. K. Salomon, M. A. Caporizzo, S. Curry, N. A. Kelly, K. Bedi, A. I. Bogush, E. Kramer, S. Schlossarek, P. Janiak, M. J. Moutin, L. Carrier, K. B. Margulies and B. L. Prosser (2020). "Depletion of Vasohibin 1 Speeds Contraction and Relaxation in Failing Human Cardiomyocytes." Circ Res **127**(2): e14-e27.
16. Elliott, P., B. Andersson, E. Arbustini, Z. Bilinska, F. Cecchi, P. Charron, O. Dubourg, U. Kuhl, B. Maisch, W. J. McKenna, L. Monserrat, S. Pankuweit, C. Rapezzi, P. Seferovic, L. Tavazzi and A. Keren (2008). "Classification of the cardiomyopathies: a position statement from the European Society Of Cardiology Working Group on Myocardial and Pericardial Diseases." Eur Heart J **29**(2): 270-276.
17. Elliott, P. and W. J. McKenna (2004). "Hypertrophic cardiomyopathy." Lancet **363**(9424): 1881-1891.
18. Factor, S. M., J. Butany, M. J. Sole, E. D. Wigle, W. C. Williams and M. Rojkind (1991). "Pathologic fibrosis and matrix connective tissue in the subaortic myocardium of patients with hypertrophic cardiomyopathy." J Am Coll Cardiol **17**(6): 1343-1351.
19. Fonrose, X., F. Ausseil, E. Soleilhac, V. Masson, B. David, I. Pouny, J. C. Cintrat, B. Rousseau, C. Barette, G. Massiot and L. Lafanechere (2007). "Parthenolide inhibits tubulin carboxypeptidase activity." Cancer Res **67**(7): 3371-3378.
20. Fougerousse, F., A. L. Delezoide, M. Y. Fiszman, K. Schwartz, J. S. Beckmann and L. Carrier (1998). "Cardiac myosin binding protein C gene is specifically expressed in heart during murine and human development." Circ Res **82**(1): 130-133.
21. Fraysse, B., F. Weinberger, S. C. Bardswell, F. Cuello, N. Vignier, B. Geertz, J. Starbatty, E. Kramer, C. Coirault, T. Eschenhagen, J. C. Kentish, M. Avkiran and L. Carrier (2012). "Increased myofilament Ca²⁺ sensitivity and diastolic dysfunction as early consequences of Mybpc3 mutation in heterozygous knock-in mice." J Mol Cell Cardiol **52**(6): 1299-1307.
22. Gedicke-Hornung, C., V. Behrens-Gawlik, S. Reischmann, B. Geertz, D. Stimpel, F. Weinberger, S. Schlossarek, G. Precigout, I. Braren, T. Eschenhagen, G. Mearini, S. Lorain, T. Voit, P. A. Dreyfus, L. Garcia and L. Carrier (2013). "Rescue of cardiomyopathy through U7snRNA-mediated exon skipping in Mybpc3-targeted knock-in mice." EMBO Mol Med **5**(7): 1128-1145.
23. Ghantous, A., A. Sinjab, Z. Herceg and N. Darwiche (2013). "Parthenolide: from plant shoots to cancer roots." Drug Discov Today **18**(17-18): 894-905.
24. Girolami, F., I. Olivetto, I. Passerini, E. Zachara, S. Nistri, F. Re, S. Fantini, K. Baldini, F. Torricelli and F. Cecchi (2006). "A molecular screening strategy based on beta-myosin heavy chain, cardiac myosin binding protein C and troponin T genes in Italian patients with hypertrophic cardiomyopathy." J Cardiovasc Med (Hagerstown) **7**(8): 601-607.
25. Goodson, H. V. and E. M. Jonasson (2018). "Microtubules and Microtubule-Associated Proteins." Cold Spring Harb Perspect Biol **10**(6).
26. Gundersen, G. G., S. Khawaja and J. C. Bulinski (1987). "Postpolymerization detyrosination of alpha-tubulin: a mechanism for subcellular differentiation of microtubules." J Cell Biol **105**(1): 251-264.
27. Hallak, M. E., J. A. Rodriguez, H. S. Barra and R. Caputto (1977). "Release of tyrosine from tyrosinated tubulin. Some common factors that affect this process and the assembly of tubulin." FEBS Lett **73**(2): 147-150.
28. Harris, S. P., R. G. Lyons and K. L. Bezold (2011). "In the thick of it: HCM-causing mutations in myosin binding proteins of the thick filament." Circ Res **108**(6): 751-764.

29. Hoffman, L. M., M. A. Smith, C. C. Jensen, M. Yoshigi, E. Blankman, K. S. Ullman and M. C. Beckerle (2020). "Mechanical stress triggers nuclear remodeling and the formation of transmembrane actin nuclear lines with associated nuclear pore complexes." Mol Biol Cell **31**(16): 1774-1787.
30. Janke, C. and J. C. Bulinski (2011). "Post-translational regulation of the microtubule cytoskeleton: mechanisms and functions." Nat Rev Mol Cell Biol **12**(12): 773-786.
31. Kerr, J. P., P. Robison, G. Shi, A. I. Bogush, A. M. Kempema, J. K. Hexum, N. Becerra, D. A. Harki, S. S. Martin, R. Raiteri, B. L. Prosser and C. W. Ward (2015). "Detyrosinated microtubules modulate mechanotransduction in heart and skeletal muscle." Nat Commun **6**: 8526.
32. Kirschner, M. and T. Mitchison (1986). "Beyond self-assembly: from microtubules to morphogenesis." Cell **45**(3): 329-342.
33. Kreitzer, G., G. Liao and G. G. Gundersen (1999). "Detyrosination of tubulin regulates the interaction of intermediate filaments with microtubules in vivo via a kinesin-dependent mechanism." Mol Biol Cell **10**(4): 1105-1118.
34. Kushner, J. S., G. Liu, R. J. Eisert, G. A. Bradshaw, G. S. Pitt, J. T. Hinson, M. Kalocsay and S. O. Marx (2022). "Detecting Cardiovascular Protein-Protein Interactions by Proximity Proteomics." Circ Res **130**(2): 273-287.
35. Litvinukova, M., C. Talavera-Lopez, H. Maatz, D. Reichart, C. L. Worth, E. L. Lindberg, M. Kanda, K. Polanski, M. Heinig, M. Lee, E. R. Nadelmann, K. Roberts, L. Tuck, E. S. Fasouli, D. M. DeLaughter, B. McDonough, H. Wakimoto, J. M. Gorham, S. Samari, K. T. Mahbubani, K. Saeb-Parsy, G. Patone, J. J. Boyle, H. Zhang, H. Zhang, A. Viveiros, G. Y. Oudit, O. A. Bayraktar, J. G. Seidman, C. E. Seidman, M. Nosedá, N. Hubner and S. A. Teichmann (2020). "Cells of the adult human heart." Nature **588**(7838): 466-472.
36. Mann, S. S. and J. A. Hammarback (1994). "Molecular characterization of light chain 3. A microtubule binding subunit of MAP1A and MAP1B." J Biol Chem **269**(15): 11492-11497.
37. Maron, B. J., J. M. Gardin, J. M. Flack, S. S. Gidding, T. T. Kurosaki and D. E. Bild (1995). "Prevalence of hypertrophic cardiomyopathy in a general population of young adults. Echocardiographic analysis of 4111 subjects in the CARDIA Study. Coronary Artery Risk Development in (Young) Adults." Circulation **92**(4): 785-789.
38. Maron, B. J., S. R. Ommen, C. Semsarian, P. Spirito, I. Olivetto and M. S. Maron (2014). "Hypertrophic cardiomyopathy: present and future, with translation into contemporary cardiovascular medicine." J Am Coll Cardiol **64**(1): 83-99.
39. Marston, S., O. Copeland, K. Gehmlich, S. Schlossarek and L. Carrier (2012). "How do MYBPC3 mutations cause hypertrophic cardiomyopathy?" J Muscle Res Cell Motil **33**(1): 75-80.
40. Marston, S., O. Copeland, A. Jacques, K. Livesey, V. Tsang, W. J. McKenna, S. Jalilzadeh, S. Carballo, C. Redwood and H. Watkins (2009). "Evidence from human myectomy samples that MYBPC3 mutations cause hypertrophic cardiomyopathy through haploinsufficiency." Circ Res **105**(3): 219-222.
41. McKenna, W. J. and D. P. Judge (2021). "Epidemiology of the inherited cardiomyopathies." Nat Rev Cardiol **18**(1): 22-36.
42. Mearini, G., D. Stimpel, B. Geertz, F. Weinberger, E. Kramer, S. Schlossarek, J. Mourot-Filiatre, A. Stoehr, A. Dutsch, P. J. Wijnker, I. Braren, H. A. Katus, O. J. Muller, T. Voit, T. Eschenhagen and L. Carrier (2014). "Mybpc3 gene therapy for neonatal cardiomyopathy enables long-term disease prevention in mice." Nat Commun **5**: 5515.
43. Mearini, G., D. Stimpel, E. Kramer, B. Geertz, I. Braren, C. Gedicke-Hornung, G. Precigout, O. J. Muller, H. A. Katus, T. Eschenhagen, T. Voit, L. Garcia, S. Lorain and L. Carrier (2013). "Repair

- of Mybpc3 mRNA by 5'-trans-splicing in a Mouse Model of Hypertrophic Cardiomyopathy." Mol Ther Nucleic Acids **2**: e102.
44. Mitchison, T. and M. Kirschner (1984). "Dynamic instability of microtubule growth." Nature **312**(5991): 237-242.
45. Moolman-Smook, J., E. Flashman, W. de Lange, Z. Li, V. Corfield, C. Redwood and H. Watkins (2002). "Identification of novel interactions between domains of Myosin binding protein-C that are modulated by hypertrophic cardiomyopathy missense mutations." Circ Res **91**(8): 704-711.
46. Morita, H., H. L. Rehm, A. Menesses, B. McDonough, A. E. Roberts, R. Kucherlapati, J. A. Towbin, J. G. Seidman and C. E. Seidman (2008). "Shared genetic causes of cardiac hypertrophy in children and adults." N Engl J Med **358**(18): 1899-1908.
47. Nimmagadda, S., P. Geetha-Loganathan, F. Prots, M. Scaal, B. Christ and R. Huang (2007). "Expression pattern of Vasohibin during chick development." Dev Dyn **236**(5): 1358-1362.
48. Nunes, P., T. Hernandez, I. Roth, X. Qiao, D. Strebel, R. Bouley, A. Charollais, P. Ramadori, M. Foti, P. Meda, E. Feraille, D. Brown and U. Hasler (2013). "Hypertonic stress promotes autophagy and microtubule-dependent autophagosomal clusters." Autophagy **9**(4): 550-567.
49. O'Connell, T. D., M. C. Rodrigo and P. C. Simpson (2007). "Isolation and culture of adult mouse cardiac myocytes." Methods Mol Biol **357**: 271-296.
50. Offer, G., C. Moos and R. Starr (1973). "A new protein of the thick filaments of vertebrate skeletal myofibrils. Extractions, purification and characterization." J Mol Biol **74**(4): 653-676.
51. Ommen, S. R., S. Mital, M. A. Burke, S. M. Day, A. Deswal, P. Elliott, L. L. Evanovich, J. Hung, J. A. Joglar, P. Kantor, C. Kimmelstiel, M. Kittleson, M. S. Link, M. S. Maron, M. W. Martinez, C. Y. Miyake, H. V. Schaff, C. Semsarian and P. Sorajja (2020). "2020 AHA/ACC Guideline for the Diagnosis and Treatment of Patients With Hypertrophic Cardiomyopathy: A Report of the American College of Cardiology/American Heart Association Joint Committee on Clinical Practice Guidelines." Circulation **142**(25): e558-e631.
52. Pohlmann, L., I. Kroger, N. Vignier, S. Schlossarek, E. Kramer, C. Coirault, K. R. Sultan, A. El-Armouche, S. Winegrad, T. Eschenhagen and L. Carrier (2007). "Cardiac myosin-binding protein C is required for complete relaxation in intact myocytes." Circ Res **101**(9): 928-938.
53. Prosser, S. L. and L. Pelletier (2017). "Mitotic spindle assembly in animal cells: a fine balancing act." Nat Rev Mol Cell Biol **18**(3): 187-201.
54. Raybin, D. and M. Flavin (1977). "Enzyme which specifically adds tyrosine to the alpha chain of tubulin." Biochemistry **16**(10): 2189-2194.
55. Richard, P., P. Charron, L. Carrier, C. Ledeuil, T. Cheav, C. Pichereau, A. Benaiche, R. Isnard, O. Dubourg, M. Burban, J. P. Gueffet, A. Millaire, M. Desnos, K. Schwartz, B. Hainque, M. Komajda and E. H. F. Project (2003). "Hypertrophic cardiomyopathy: distribution of disease genes, spectrum of mutations, and implications for a molecular diagnosis strategy." Circulation **107**(17): 2227-2232.
56. Robison, P., M. A. Caporizzo, H. Ahmadzadeh, A. I. Bogush, C. Y. Chen, K. B. Margulies, V. B. Shenoy and B. L. Prosser (2016). "Detyrosinated microtubules buckle and bear load in contracting cardiomyocytes." Science **352**(6284): aaf0659.
57. Roux, K. J., D. I. Kim, B. Burke and D. G. May (2018). "BioID: A Screen for Protein-Protein Interactions." Curr Protoc Protein Sci **91**: 19 23 11-19 23 15.
58. Roux, K. J., D. I. Kim, M. Raida and B. Burke (2012). "A promiscuous biotin ligase fusion protein identifies proximal and interacting proteins in mammalian cells." J Cell Biol **196**(6): 801-810.

59. Salomon, A. K., S. A. Phyto, N. Okami, J. Heffler, P. Robison, A. I. Bogush and B. L. Prosser (2022). "Desmin intermediate filaments and tubulin detyrosination stabilize growing microtubules in the cardiomyocyte." Basic Res Cardiol **117**(1): 53.
60. Samavarchi-Tehrani, P., R. Samson and A. C. Gingras (2020). "Proximity Dependent Biotinylation: Key Enzymes and Adaptation to Proteomics Approaches." Mol Cell Proteomics **19**(5): 757-773.
61. Sanchez, A. D. and J. L. Feldman (2017). "Microtubule-organizing centers: from the centrosome to non-centrosomal sites." Curr Opin Cell Biol **44**: 93-101.
62. Schlossarek, S., G. Mearini and L. Carrier (2011). "Cardiac myosin-binding protein C in hypertrophic cardiomyopathy: mechanisms and therapeutic opportunities." J Mol Cell Cardiol **50**(4): 613-620.
63. Schuldt, M., J. Pei, M. Harakalova, L. M. Dorsch, S. Schlossarek, M. Mokry, J. C. Knol, T. V. Pham, T. Schelfhorst, S. R. Piersma, C. Dos Remedios, M. Dalinghaus, M. Michels, F. W. Asselbergs, M. J. Moutin, L. Carrier, C. R. Jimenez, J. van der Velden and D. W. D. Kuster (2021). "Proteomic and Functional Studies Reveal Detyrosinated Tubulin as Treatment Target in Sarcomere Mutation-Induced Hypertrophic Cardiomyopathy." Circ Heart Fail **14**(1): e007022.
64. Shirani, J., R. Pick, W. C. Roberts and B. J. Maron (2000). "Morphology and significance of the left ventricular collagen network in young patients with hypertrophic cardiomyopathy and sudden cardiac death." J Am Coll Cardiol **35**(1): 36-44.
65. Thottakara, T., F. W. Friedrich, S. Reischmann, S. Braumann, S. Schlossarek, E. Kramer, D. Juhr, H. Schluter, J. van der Velden, J. Munch, M. Patten, T. Eschenhagen, C. Moog-Lutz and L. Carrier (2015). "The E3 ubiquitin ligase Asb2beta is downregulated in a mouse model of hypertrophic cardiomyopathy and targets desmin for proteasomal degradation." J Mol Cell Cardiol **87**: 214-224.
66. van der Velden, J., C. Y. Ho, J. C. Tardiff, I. Olivotto, B. C. Knollmann and L. Carrier (2015). "Research priorities in sarcomeric cardiomyopathies." Cardiovasc Res **105**(4): 449-456.
67. Vignier, N., S. Schlossarek, B. Fraysse, G. Mearini, E. Kramer, H. Pointu, N. Mougnot, J. Guiard, R. Reimer, H. Hohenberg, K. Schwartz, M. Vernet, T. Eschenhagen and L. Carrier (2009). "Nonsense-mediated mRNA decay and ubiquitin-proteasome system regulate cardiac myosin-binding protein C mutant levels in cardiomyopathic mice." Circ Res **105**(3): 239-248.
68. Wen, J., K. R. You, S. Y. Lee, C. H. Song and D. G. Kim (2002). "Oxidative stress-mediated apoptosis. The anticancer effect of the sesquiterpene lactone parthenolide." J Biol Chem **277**(41): 38954-38964.
69. Winegrad, S. (1999). "Cardiac myosin binding protein C." Circ Res **84**(10): 1117-1126.
70. Yamamoto, K. and C. Moos (1983). "The C-proteins of rabbit red, white, and cardiac muscles." J Biol Chem **258**(13): 8395-8401.
71. Zebrowski, D. C., S. Vergarajauregui, C. C. Wu, T. Piatkowski, R. Becker, M. Leone, S. Hirth, F. Ricciardi, N. Falk, A. Giessl, S. Just, T. Braun, G. Weidinger and F. B. Engel (2015). "Developmental alterations in centrosome integrity contribute to the post-mitotic state of mammalian cardiomyocytes." Elife **4**.
72. Zou, Y., L. Song, Z. Wang, A. Ma, T. Liu, H. Gu, S. Lu, P. Wu, Y. Zhang dagger, L. Shen dagger, Y. Cai, Y. Zhen double dagger, Y. Liu and R. Hui (2004). "Prevalence of idiopathic hypertrophic cardiomyopathy in China: a population-based echocardiographic analysis of 8080 adults." Am J Med **116**(1): 14-18.

8 Acknowledgements

The completion of this experimental medical thesis marks the finalization of an arduous yet rewarding, maybe slightly prolonged journey, and I owe my gratitude to several people who have played pivotal roles in its realization.

Foremost, I express my deepest thankfulness to Prof. Dr. Lucie Carrier, whose leadership and mentorship have been the cornerstone of this endeavor. Her intellectual guidance, insightful feedback, and unwavering support have not only shaped the direction of this research but have also been instrumental in fostering an environment conducive to scientific exploration.

Another crucial person in the development of this thesis is Dr. Saskia Schlossarek. Her wonderful supervision and dedication towards the project ensured my method-specific understanding needed at every step of the way while enhancing the quality of this work in its foundation. In times of concern, she provided great optimism and solution-oriented suggestions of which I am dearly thankful.

I further want to thank Prof. Dr. Thomas Eschenhagen for the opportunity to work on my medical thesis in the Department of Experimental Pharmacology and Toxicology, University Medical Centre, Hamburg-Eppendorf. His thoughtful and precise annotations, during my brief project presentations within the laboratory, were often spark to new perspectives and directions for this work.

Equally deserving of acknowledgment are my friends as well as my laboratory partners and Co-workers, surpassing the AG Carrier. Here especially to mention: Annabell Ottenberg, and Antonia Zech, whose camaraderie and companionship have been a source of solace and strength throughout this journey. The shared experiences, late-night discussions, and collective celebrations of milestones created a support network that transcended the confines of academia. Further, without the likes of Lisa Krämer and her support and effort towards the final steps of the project, this work would have looked very different from what it does now. Moreover, I want to mention all the other people who participated and supported me during my time at the lab, creating a supportive, friendly and simply unique atmosphere within the research group: Frederik Flenner, Maksimilian Prondzynski, Silke Düsener, Birgit Geertz, Giulia Mearini. The bonds forged

with friends during this period are a testament to the importance of community in navigating the challenges of scientific exploration.

I extend gratitude to the Cardiovascular Research Center (CVRC) for providing an enriching environment conducive to my studies. The supportive community of researchers, clinicians, and staff has created a dynamic and inspiring atmosphere that significantly contributed to the success of this thesis.

The journey through this thesis has been enriched by the unwavering support of my family, to whom I owe an immense debt of gratitude. Their emotional support, love and unflagging encouragement have been the bedrock upon which this academic pursuit stands. Their belief in my capabilities has been a driving force, motivating me to overcome obstacles and persevere through the complexities inherent in medical education, research and as a medical practitioner.

Lastly, I express my deepest gratitude to my parents to whom I am forever grateful for everything they made possible; this medical thesis is dedicated to them.

9 Curriculum Vitae

Personal Data

Name: Alexander Georgios Tourounoglou
Date of Birth: 04th October 1994
Place of Birth: Hamburg, Germany

Education

2012 Abitur, Helene-Lange-Gymnasium, Hamburg
2012 – 2013 General Engineering Science, Technical University Hamburg-Harburg
2013 – 2021 Medicine, University Hamburg
04/2016 1st Medical Examinations, Hamburg
10/2016 – 10/2017 MD scholarship student, Cardiovascular Research Center, Institute for Pharmacology and Toxicology (Research group of Prof. Dr. Lucie Carrier), Hamburg
04/2020 2nd Medical Examinations, Hamburg
05/2021 3rd Medical Examinations, Hamburg
05-09/2020 Practical year, Cardiology, intensive care unit and internal medicine, Albertinen Krankenhaus, Hamburg
09-12/2020 Practical year, Paediatrics, Katholisches Kinderkrankenhaus Wilhelstift, Hamburg
12/2020 – 04/2021 Practical year, Visceral and orthopedic surgery, Städtisches Klinikum Lüneburg, Lüneburg

Clinical experience

Since 11/2021 Resident at the Department of Cardiology, Herz- und Gefäßzentrum, Albertinen Krankenhaus, Hamburg

10 Appendix

10.1. List of abbreviations

°C	Degree Celsius
4-(2-hydroxyethyl)-1-piperazineethanesulfonicacid	HEPES
A	Adenine
AMCM	Adult mouse cardiomyocyte
APS	Ammonium persulfate
ARVC	Arrhythmogenic right ventricular cardiomyopathy
ATP	adenosinetriphospate
BDM	2,3-butanedione monoxime
BSA	Bovine serum albumin
Ca ²⁺	Calcium
CaCl ₂	Calcium chloride
cMRI	Cardiac magnetic resonance imaging
cMyBP-C	cardiac myosin-binding protein C
CO ₂	Carbon dioxide
CT	computed tomography
cTnC	cardiac troponin C
cTnI	cardiac troponin I
cTnT	cardiac troponin T
DAPI	4',6-diamidino-2-phenylidole
DCM	Dilated cardiomyopathy
DPBS	Dulbecco's phosphate-buffered saline
DTT	Dithiothreitol
EDTA	Ethylenediaminetetraacetic acid
ESC	European Society of Cardiology'
FCS	fetal calf serum
G	Guanine
g	Gram
H ₂ O	Water
HCL	Hydrogen chloride

HCM	Hypertrophic cardiomyopathy
HF	Heart failure
Hz	Hertz
IF	Immunofluorescence
Ig	Immunoglobulin
ITS	Insulin-Transferrin-Selenium
KCl	Potassium chloride
kDa	Kilodalton
KH_2PO_4	Potassium phosphate
KHCO_3	Potassium hydrogen carbonate
KI	Knock-in
KO	Knock-out
l	Liter
LC3	Microtubule-associated protein light-chain 3
LMM	Light meromyosin
LV	Left ventricular
LV-EF	Left ventricular ejection fraction
LVOTO	Left ventricular outflow obstruction
m	Meter
M	Molar
MC-CM	Cell culture medium
MgSO_4	Magnesium sulfate
min	Minute
M-Motif	MyBP-C motif
mRNA	Messenger ribonucleic acid
MVT	Murine ventricular tissue
Na_2HPO_4	Di-Sodium hydrogen phosphate
NaCl	Sodium chloride
NaF	Sodium fluoride
NaHCO_3	Sodium hydrogen carbonate
ncMTOCs	Non-centrosomal microtubule-organizing centres
NCX	Sodium-calcium exchanger
PBS	Phosphate buffered saline

PFA	Paraformaldehyde
PLA	Proximity ligation assay
PTL	Parthenolide
PTM	Post-translational modification
RCM	Restrictive cardiomyopathy
RNA	Ribonucleic acid
SDS-PAGE	Sodium dodecyl sulfate polyacrylamide gel electrophoresis
SERCA	Sarco/endoplasmic reticulum Ca ²⁺ -ATPase
SRX	Super-relaxed
SVBP	Small vasohibin-binding protein
TCP	Tubulin carboxypeptidase
Temed	Tetramethyl ethylenediamine
TTL	Tubulin-tyrosine ligase
V	Volt
VASH	Vasohibin
WB	Western Blot
WT	Wild-type
β-MHC	β-myosin heavy chain

10.2. SI Prefixes

k	Kilo (10 ³)
m	Mili (10 ⁻³)
μ	Micro (10 ⁻⁶)
n	Nano (10 ⁻⁹)

10.3. Protocol PLA Analysis

10.3.1. Analysis of cell area with ImageJ / FIJI

Use the ImageJ Program with the FIJI expansion package. This protocol can only be used for 2D pictures.

1. Add image (".czi-file") to ImageJ (via drag&drop). The picture needs a scale bar which can be added directly when taking the picture in the imaging software (ZEN).
2. Zoom in to scale bar and draw a line matching the length of the scale bar.
3. Click 'Analyze' → 'Measure' → 'Length' (in pixels)
4. Then click 'Analyze' again → Set scale
 - a. Add measured number of pixels and known length of scale into the table
 - b. Set unit
5. To measure the cell area:
6. Click: 'Image' → 'Adjust' → Threshold: Default, Over/Under, Dark background (x), stack histogram ()
7. Lower the threshold until whole cell is visible
8. Use 'wand' (tracing)-tool to select the total cell area
9. Click 'Analyze' → Measure
10. This will provide you with the total cell area

10.3.2. PLA signal count in ImageJ

1. Add '.JPG'-picture to FIJI
2. Open color threshold / 'Image' → 'Adjust' → 'Color Threshold'
 - a. Change threshold color to 'white'
 - b. Threshold method: Default
 - c. Color space: RGB
 - d. Dark background: (x)
3. Adjust colors so that only the PLA signals are selected (visual control)
4. Press 'Select'
5. Now 'Analyze' → 'Analyze particles'
 - a. Size (pixel²)
 - b. Circularity: 0.00-1.00
 - c. Show: nothing
 - d. Display results (x)
 - e. Clear results (x)

f. Add to manager (x)

- ➔ Now all signals in the picture are counted and measured
- ➔ To select a certain area to be counted, use 'Freehand selection' and circle the area of interest
- ➔ Then 'Analyze' → 'Analyze particles'
- ➔ This gives you a table including the total signal intensity within your area of interest

Now a ratio of PLA signal to total cell area can be created allowing a quantification of the visual results.

11 Eidesstattliche Versicherung

Ich versichere ausdrücklich, dass ich die Arbeit selbständig und ohne fremde Hilfe verfasst, andere als die von mir angegebenen Quellen und Hilfsmittel nicht benutzt und die aus den benutzten Werken wörtlich oder inhaltlich entnommenen Stellen einzeln nach Ausgabe (Auflage und Jahr des Erscheinens), Band und Seite des benutzten Werkes kenntlich gemacht habe.

Ferner versichere ich, dass ich die Dissertation bisher nicht einem Fachvertreter an einer anderen Hochschule zur Überprüfung vorgelegt oder mich anderweitig um Zulassung zur Promotion beworben habe.

Ich erkläre mich einverstanden, dass meine Dissertation vom Dekanat der Medizinischen Fakultät mit einer gängigen Software zur Erkennung von Plagiaten überprüft werden kann.

Unterschrift: